European Journal of Neuroscience, Vol. 18, pp. 239–257, 2003

Endogenous rhythm generation in the pre-Bötzinger complex and ionic currents: modelling and *in vitro* studies

Ilya A. Rybak,[1] Natalia A. Shevtsova,[1] Walter M. St-John,[2] Julian F. R. Paton[3] and Olivier Pierrefiche[4]
[1]School of Biomedical Engineering, Science and Health Systems, Drexel University, Philadelphia, PA 19104, USA
[2]Department of Physiology, Dartmouth Medical School, Lebanon NH 03756, USA
[3]Department of Physiology, School of Medical Sciences, University of Bristol, Bristol BS8 1TD, UK
[4]ETP-APC, Laboratoire de Neurophysiologie, UFR de Médecine, 3 Rue des Louvels, Amiens 80036, France

Keywords: computational modelling, potassium channels, rat, respiratory rhythm, transverse slices

Abstract

The pre-Bötzinger complex is a small region in the mammalian brainstem involved in generation of the respiratory rhythm. As shown *in vitro*, this region, under certain conditions, can generate endogenous rhythmic bursting activity. Our investigation focused on the conditions that may induce this bursting behaviour. A computational model of a population of pacemaker neurons in the pre-Bötzinger complex was developed and analysed. Each neuron was modelled in the Hodgkin–Huxley style and included persistent sodium and delayed-rectifier potassium currents. We found that the firing behaviour of the model strongly depended on the expression of these currents. Specifically, bursting in the model could be induced by a suppression of delayed-rectifier potassium current (either directly or via an increase in extracellular potassium concentration, $[K^+]_o$) or by an augmentation of persistent sodium current. To test our modelling predictions, we recorded endogenous population activity of the pre-Bötzinger complex and activity of the hypoglossal (XII) nerve from *in vitro* transverse brainstem slices (700 μm) of neonatal rats (P0–P4). Rhythmic activity was absent at 3 mM $[K^+]_o$ but could be triggered by either the elevation of $[K^+]_o$ to 5–7 mM or application of potassium current blockers (4-AP, 50–200 μM, or TEA, 2 or 4 mM), or by blocking aerobic metabolism with NaCN (2 mM). This rhythmic activity could be abolished by the persistent sodium current blocker riluzole (25 or 50 μM). These findings are discussed in the context of the role of endogenous bursting activity in the respiratory rhythm generation *in vivo* vs. *in vitro* and during normal breathing *in vivo* vs. gasping.

Introduction

The pre-Bötzinger complex (pBC) is a small region in the rostroventrolateral medulla and is considered an important part of the brainstem respiratory neural network (Smith *et al*., 1991; Rekling & Feldman, 1998; Gray *et al*., 2001). As shown *in vitro*, this region, under certain conditions, can generate intrinsic rhythmic bursting activity (Johnson *et al*., 1994; Smith *et al*., 1991; Rekling & Feldman, 1998; Koshiya & Smith, 1999; Thoby-Brisson & Ramirez, 2001) which is resistant to blockade of synaptic inhibition (Feldman & Smith, 1989; Shao & Feldman, 1997). It has been suggested that this *in vitro* activity is driven by a subpopulation of pacemaker neurons located in the pBC (Smith, 1997; Butera *et al*., 1999a,b; Koshiya & Smith, 1999; Del Negro *et al*., 2001). The theoretical analysis of possible intrinsic cellular mechanisms led to the conclusion that persistent sodium currents are necessary for the generation of the endogenous rhythm in the pBC (Butera *et al*., 1999a; for an opposite view see Del Negro *et al*., 2002b). This current was recently described in pBC neurons (Koshiya *et al*., 2001; McCrimmon *et al*., 2001; Del Negro *et al*., 2002a; Shevtsova *et al*., 2002; Rybak *et al*., 2003) and its voltage-dependent properties were characterized (Del Negro *et al*., 2002a; Shevtsova *et al*., 2002; Rybak *et al*., 2003).

The role of endogenous oscillations recorded from the pBC *in vitro* in the generation of the normal ('eupnoeic') respiratory rhythm *in vivo* is still unclear. Some investigators believe that pBC pacemaker neurons form a 'kernel' of the respiratory network, producing a basic rhythm which is necessary for generation of the eupnoeic respiratory pattern (Smith, 1997; Rekling & Feldman, 1998; Butera *et al*., 1999a,b; Del Negro *et al*., 2001; Gray *et al*., 2001). Another point of view is that the pBC is only a part of the brainstem respiratory network and that neurogenesis of endogenous rhythmic activity observed *in vitro* differs from the network-based mechanisms of eupnoea, being more like the neurogenesis of gasping (Fukuda, 2000; St-John, 1996, 1998; St-John *et al*., 2002). Moreover, the neural mechanisms responsible for generation of the respiratory rhythm may be state-dependent. In frames of the 'kernel concept', Smith and colleagues considered the possibility of state-dependent transformations between mechanisms for rhythm generation (Smith, 1997; Smith *et al*., 2000). Specifically, it was suggested that both eupnoeic and gasping inspiratory patterns originate from the pBC and represent different activity states (Smith *et al*., 2000). According to the 'switching concept' (Rybak *et al*., 2001, 2002; St-John *et al*., 2002), the respiratory rhythm may be generated, depending on the conditions, by either a network mechanism operating in the entire pontomedullary network (eupnoea), or a hybrid mechanism with a pacemaker-driven kernel in the pBC (gasping). In this concept, the pBC does not perform an exclusive 'kernel' function during eupnoea, but is considered a region responsible for switching respiratory rhythmogenesis from a network-based mechanism of eupnoea to a pacemaker-driven mechanism of gasping.

In this context, it is necessary to investigate the conditions which define the generation of pacemaker-driven oscillations in the pBC

Correspondence: Dr Ilya A. Rybak, as above.
E-mail: rybak@cbis.ece.drexel.edu

Received 28 October 2002, revised 22 April 2003, accepted 1 May 2003

doi:10.1046/j.1460-9568.2003.02739.x

in vitro and compare these conditions to those occurring during gasping *in vivo*. Recent modelling studies (Rybak *et al*., 2001, 2002) suggested that the release of pacemaker-driven oscillations might be induced at the cellular level by a suppression of voltage-gated potassium currents or an augmentation of persistent sodium currents. Therefore, the major objective of the present interdisciplinary study was to investigate the role of the voltage-gated potassium and persistent sodium currents in triggering endogenous bursting activity in the pBC.

Materials and methods

Modelling methods

Single-neuron model

Our model of the pBC single pacemaker neuron is a single-compartment neuron model developed in the Hodgkin–Huxley style. This model is actually a modified version of the previous models by Butera *et al*. (1999a; Model 1) and Del Negro *et al*. (2001). The following ionic currents (and the corresponding channel conductances) were incorporated in the model: fast sodium (I_{Naf} with maximal conductance $\bar{g}_{\mathrm{Naf}}$); persistent sodium (I_{NaP} with maximal conductance $\bar{g}_{\mathrm{NaP}}$); delayed-rectifier potassium (I_{K} with maximal conductance $\bar{g}_{\mathrm{K}}$); leakage (I_{leak} with constant conductance g_{leak}), and synaptic excitatory (I_{synE} with conductance g_{synE}) and inhibitory (I_{synI} with conductance g_{synI}). These currents together define the dynamics of the neuronal membrane potential V:

$$C \cdot \mathrm{d}V/\mathrm{d}t = -I_{\mathrm{Naf}} - I_{\mathrm{NaP}} - I_{\mathrm{K}} - I_{\mathrm{leak}} - I_{\mathrm{synE}} - I_{\mathrm{synI}} \quad (1)$$

where C is the whole-cell capacitance and t is time.

Inhibitory synaptic inputs were not applied in the present study. Therefore, in all simulations described in this paper, $I_{\mathrm{synI}} = 0$.

The ionic currents were described as follows.

$$I_{\mathrm{Naf}} = \bar{g}_{\mathrm{Naf}} \cdot m^3{}_{\mathrm{Naf}} \cdot h_{\mathrm{Naf}} \cdot (V - E_{\mathrm{Na}})$$

$$I_{\mathrm{NaP}} = \bar{g}_{\mathrm{NaP}} \cdot m_{\mathrm{NaP}} \cdot h_{\mathrm{NaP}} \cdot (V - E_{\mathrm{Na}})$$

$$I_{\mathrm{K}} = \bar{g}_{\mathrm{K}} \cdot m^4_{\mathrm{K}} \cdot (V - E_{\mathrm{K}})$$

$$I_{\mathrm{leak}} = g_{\mathrm{leak}} \cdot (V - E_{\mathrm{leak}})$$

$$I_{\mathrm{synE}} = g_{\mathrm{synE}} \cdot (V - E_{\mathrm{synE}}) \quad (2)$$

Activation and inactivation of the voltage-gated channel i (e.g. fast sodium, Naf, persistent sodium, NaP, or delayed-rectifier potassium, K) were described by the following differential equations:

$$\tau_{mi}(V) \cdot \mathrm{d}m_i/\mathrm{d}t = m_{\infty i}(V) - m_i$$

$$\tau_{hi}(V) \cdot \mathrm{d}h_i/\mathrm{d}t = h_{\infty i}(V) - h_i \quad (3)$$

where the steady-state voltage-dependent activation and inactivation were described as follows.

$$m_{\infty i}(V) = (1 + \exp(-(V - V_{1/2mi})/k_{mi}))^{-1}$$

$$h_{\infty i}(V) = (1 + \exp((V - V_{1/2hi})/k_{hi}))^{-1} \quad (4)$$

The voltage-dependent time constants for activation and inactivation were described in the following form (see Butera *et al*., 1999a).

$$\tau_{mi}(V) = \frac{\bar{\tau}_{mi}}{\cosh((V - V_{1/2mi})/k_{\tau mi})};$$

$$\tau_{hi}(V) = \frac{\bar{\tau}_{hi}}{\cosh((V - V_{1/2hi})/k_{\tau hi})}; \quad (5)$$

In equations 4 and 5, $V_{1/2mi}$ and $V_{1/2hi}$ are, respectively, the half-maximal activation and the half-maximal inactivation voltages for the channel i, k_{mi} and k_{hi} are the corresponding slope factors of activation and inactivation for the channel i, $\bar{\tau}_{mi}$ and $\bar{\tau}_{hi}$ are the maximal time constants for the channel i activation and inactivation, respectively, and $k_{\tau mi}$ and $k_{\tau hi}$ are the corresponding slope factors for the time constants of channel i activation and inactivation.

The reversal potentials for sodium (E_{Na}) and potassium (E_{K}) channels were defined by the Nernst equation for single-valence ions:

$$E_i = \frac{R \cdot T}{F} \cdot 1\mathrm{n}\left(\frac{[\mathrm{X}_i]_{\mathrm{o}}}{[\mathrm{X}_i]_{\mathrm{in}}}\right) \quad (6)$$

where R is the universal gas constant, T is the temperature in degrees Kelvin, F is the Faraday constant, $[\mathrm{X}_i]_{\mathrm{o}}$ is the concentration of ions i outside the cell and $[\mathrm{X}_i]_{\mathrm{in}}$ is the concentration of these ions inside the cell. The reversal potential for leakage channels was described in the form of the Goldman equation for single-valence ions:

$$E_{\mathrm{leak}} = \frac{R \cdot T}{F} \cdot 1\mathrm{n}\left(\frac{[\mathrm{K}^+]_{\mathrm{o}} + p_{\mathrm{Na/K}} \cdot [\mathrm{Na}^+]_{\mathrm{o}}}{[\mathrm{K}^+]_{\mathrm{in}} + p_{\mathrm{Na/K}} \cdot [\mathrm{Na}^+]_{\mathrm{in}}}\right) \quad (7)$$

where $p_{\mathrm{Na/K}}$ is the relative permeability of Na^+ ions (with respect to permeability of K^+ ions) at rest.

The reversal potential for the excitatory (E_{synE}) synaptic channel was considered constant. The conductance of this channel g_{synE} had two components, one defining external excitatory drive to the neuron (g_{Edr}) and the other defining excitatory inputs from other neurons in the network (g_{Enet}).

$$g_{\mathrm{synE}} = g_{\mathrm{Edr}} + g_{\mathrm{Enet}} \quad (8)$$

g_{synE} was equal to zero if a neuron did not receive any excitatory inputs. For single-neuron simulations, $g_{\mathrm{Enet}} = 0$ and g_{Edr} was used as a variable defining external input to the neuron.

Population model

Synaptic interactions between the neurons in the network were simulated in the following way. At rest, the conductances of synaptic channels were zero. Each spike arriving from the neuron j to the excitatory synapse of the neuron i at the time t_{kj} increased the synaptic conductance by $\bar{g}_{\mathrm{E}} \cdot w_{ji}$, where w_{ji} is the synaptic weight of the excitatory input from neuron j to neuron i and $\bar{g}_{\mathrm{E}}$ is the parameter defining an increase in the synaptic conductance produced by one spike at $w_{ji} = 1$. The dynamics of synaptic conductance in the neuron i produced by inputs from other neurons in the network was described as follows:

$$g_{\mathrm{Eneti}}(t) = \bar{g}_{\mathrm{E}} \cdot \sum_{j(j \neq i)} w_{ji} \cdot \sum \exp(-(t - t_{kj})/\tau_{\mathrm{synE}}) \quad (9)$$

where τ_{synE} defines the inactivation time constant of the excitatory synaptic channel.

In all simulations described in this report, we considered populations of 50 neurons which were fully interconnected with excitatory synaptic connections.

Choices of model parameters

Parameters used in our simulations are shown in Table 1. All voltage-gated and kinetic parameters for the fast sodium channel (Fig. 1, A1–A3) as well as voltage-gated characteristics for the persistent sodium activation (Fig. 1, B1) were drawn from experimental studies using acutely dissociated neurons from the pBC (Shevtsova *et al*., 2002; Rybak *et al*., 2003). The experimentally estimated values for maximal conductances of the fast and persistent sodium currents in pBC neurons were 34–170 and 0.5–5.0 nS, respectively (Shevtsova *et al*., 2002; Rybak *et al*., 2003). In the model, we set the basic values of $\bar{g}_{\mathrm{Naf}} = 150.0$ nS and $\bar{g}_{\mathrm{NaP}} = 4.0$ nS. The value of maximal conductance for the persistent sodium current used in the model was consistent with the data of Koshiya *et al*. (2001) (2.4–4.5 nS) and recent data of Del Negro *et al*. (2002a), who reported that the maximal value of $\bar{g}_{\mathrm{NaP}}$ reached 4–5 nS.

The parameters of steady-state activation for the persistent sodium current in our model ($V_{1/2m\mathrm{NaP}} = -47.1$ mV, $k_{m\mathrm{NaP}} = 3.1$ mV; Table 1, Fig. 1B) were taken from the measurements in acutely dissociated, functionally unidentified pBC neurons (Shevtsova *et al*., 2002; Rybak *et al*., 2003). These parameters differed from those obtained recently by Del Negro *et al*. (2002a) in the studies of functionally identified pBC neurons ($V_{1/2m\mathrm{NaP}} = -40$ mV, $k_{m\mathrm{NaP}} = 5$ mV). We preferred to use the parameters from the former study because Del Negro and colleagues did not characterize the fast sodium current and did not separate the persistent sodium current from the noninactivating window component of the fast sodium current. Therefore in their study the measured characteristics could be related to the total noninactivating sodium current rather than to the persistent sodium current alone. At the same time, Del Negro *et al*. (2002a) showed that the steady-state characteristics of the persistent sodium current activation were not significantly different in pacemaker vs. nonpacemaker pBC cells.

Several experimental studies have demonstrated that persistent sodium channels slowly inactivate (Fleidervish & Gutnick, 1996; Fleidervish *et al*., 1996; Baker & Bostock, 1998; Magistretti & Alonso, 1999). According to these data, and similar to Model 1 by Butera *et al*. (1999a), the persistent sodium channel in our model had slow inactivation. The half-maximal inactivation voltage for the persistent sodium channel ($V_{1/2h\mathrm{NaP}} = -57.0$ mV), the slope factor for inactivation ($k_{m\mathrm{NaP}} = 3.0$ mV) and the maximal inactivation time constant ($\bar{\tau}_{\tau h\mathrm{NaP}} = 20$ s) were chosen in our preliminary simulations to produce a range of experimentally observed burst frequencies and durations (Table 1; Fig. 1, B1 and B3). The maximal time constant for activation of the persistent sodium current was assumed to be equal to that of the fast sodium channel ($\bar{\tau}_{m\mathrm{NaP}} = \bar{\tau}_{m\mathrm{Naf}}$). The slope factors for the time constants of persistent sodium channel activation and inactivation were set to be twice the slope factors for the voltage-dependent activation and inactivation, respectively ($k_{\tau m\mathrm{NaP}} = 2 \cdot k_{m\mathrm{NaP}}$ and $k_{\tau h\mathrm{NaP}} = 2 \cdot k_{h\mathrm{NaP}}$; see equations 2–4 and subsequent explanations in Butera *et al*., 1999a).

The delayed-rectifier potassium channels have not been experimentally characterized in either the pBC or other respiration-related regions. The voltage-gated characteristics for activation of this channel were taken and adapted from the model of thalamocortical neurons by McCormick & Huguenard (1992). The curve of voltage-dependent activation for delayed-rectifier potassium channel, taken from the model of McCormick & Huguenard (1992), was shifted to more negative values of voltage. The slope of this curve was modified such that the voltage-dependent activation of the delayed-rectifier potassium current in our model had the same voltage relationship (in the half-maximal activation voltage and activation threshold) with the fast sodium activation as was in the original model of McCormick & Huguenard (1992). The resultant curve of voltage-dependent activation of the delayed-rectifier potassium channel was then fitted to a Boltzmann function to define the half-maximal activation voltage and slope factor for this channel ($V_{1/2m\mathrm{K}} = -44.5$ mV; $k_{m\mathrm{K}} = 5.0$ mV; see Table 1 and Fig. 1, C1). The maximal activation time constant and the slope factor were set as follows: $\bar{\tau}_{m\mathrm{K}} = 4.0$ ms and $k_{\tau m\mathrm{K}} = 2 \cdot k_{m\mathrm{K}}$ (see Table 1 and Fig. 1, C2). The basic value of the maximal conductance of this channel was set to $\bar{g}_{\mathrm{K}} = 50.0$ nS, which was found optimal in providing a stable generation of spikes and bursts in our model. An increase in $\bar{g}_{\mathrm{K}}$ to 75 nS eliminated the ability of the neuron to generate

TABLE 1. Model parameters

Ionic channel parameters				
Fast sodium				
Activation	$V_{1/2m\mathrm{Naf}} = -43.8$ mV	$k_{m\mathrm{Naf}} = 6.0$ mV	$\tau_{m\mathrm{Naf}} = 0.9$ ms	$k_{\tau m\mathrm{Naf}} = 14.0$ mV
Inactivation	$V_{1/2h\mathrm{Naf}} = -67.5$ mV	$k_{h\mathrm{Naf}} = 10.8$ mV	$\tau_{h\mathrm{Naf}} = 35.2$ ms	$k_{\tau h\mathrm{Naf}} = 12.8$ mV
Maximal conductance	$\bar{g}_{\mathrm{Naf}} = 150$ nS			
Persistent sodium				
Activation	$V_{1/2m\mathrm{NaP}} = -47.1$ mV	$k_{m\mathrm{NaP}} = 3.1$ mV	$\tau_{m\mathrm{NaP}} = 0.9$ ms	$k_{\tau m\mathrm{NaP}} = 6.2$ mV
Inactivation	$V_{1/2h\mathrm{NaP}} = -57.0$ mV	$k_{h\mathrm{NaP}} = 3.0$ mV	$\tau_{h\mathrm{NaP}} = 20\,000$ ms	$k_{\tau h\mathrm{NaP}} = 6.0$ mV
Maximal conductance	$\bar{g}_{\mathrm{NaP}} = 4.0$ nS (basic value)			
Delayed-rectifier potassium				
Activation	$V_{1/2m\mathrm{K}} = -44.5$ mV	$k_{m\mathrm{K}} = 5.0$ mV	$\tau_{m\mathrm{K}} = 4.0$ ms	$k_{\tau m\mathrm{K}} = 10.0$ mV
Maximal conductance	$\bar{g}_{\mathrm{K}} = 50.0$ nS (basic value)			
Leakage	$g_{\mathrm{leak}} = 2.0$ nS (basic value)			
Neuron parameters				
Ionic concentrations and reversal potentials	$[\mathrm{Na}^+]_{\mathrm{in}} = 15$ mM $[\mathrm{K}^+]_{\mathrm{in}} = 140$ mM $p_{\mathrm{Na/K}} = 0.03$ $E_{\mathrm{synE}} = 0$ mV	$[\mathrm{Na}^+]_{\mathrm{o}} = 145$ mM $[\mathrm{K}^+]_{\mathrm{o}} = 3$ mM (basic value)	($E_{\mathrm{Na}} = 58.65$ mV at $T = 300$ K). ($E_{\mathrm{K}} = -99$ mV at $[\mathrm{K}^+]_{\mathrm{o}} = 3$ mM and $T = 300$ K) ($E_{\mathrm{leak}} = -76$ mV at $[\mathrm{K}^+]_{\mathrm{o}} = 3$ mM and $T = 300$ K)	
Membrane capacitance	$C = 36.2$ pF			
Network/population parameters				
Synaptic connections	$\bar{g}_{\mathrm{E}} = 0.1$ nS	$\tau_{\mathrm{synE}} = 5$ ms		
Random distribution of parameters in the population	$\bar{g}_{\mathrm{NaP}} = 4.0 \pm 0.4$ nS $w_{ij} = 0.6 \pm 0.06$	$\bar{g}_{\mathrm{K}} = 50.0 \pm 5.0$ nS $N = 50$	$g_{\mathrm{leak}} = 2.0 \pm 0.6$ nS	$g_{\mathrm{Edr}} = 0.12 \pm 0.024$ nS
Constants and other parameters	$R = 8.3143 \times 10^3$ J/(KM × K)	$F = 9.648 \times 10^4$ C/M	$T = 300$ K	

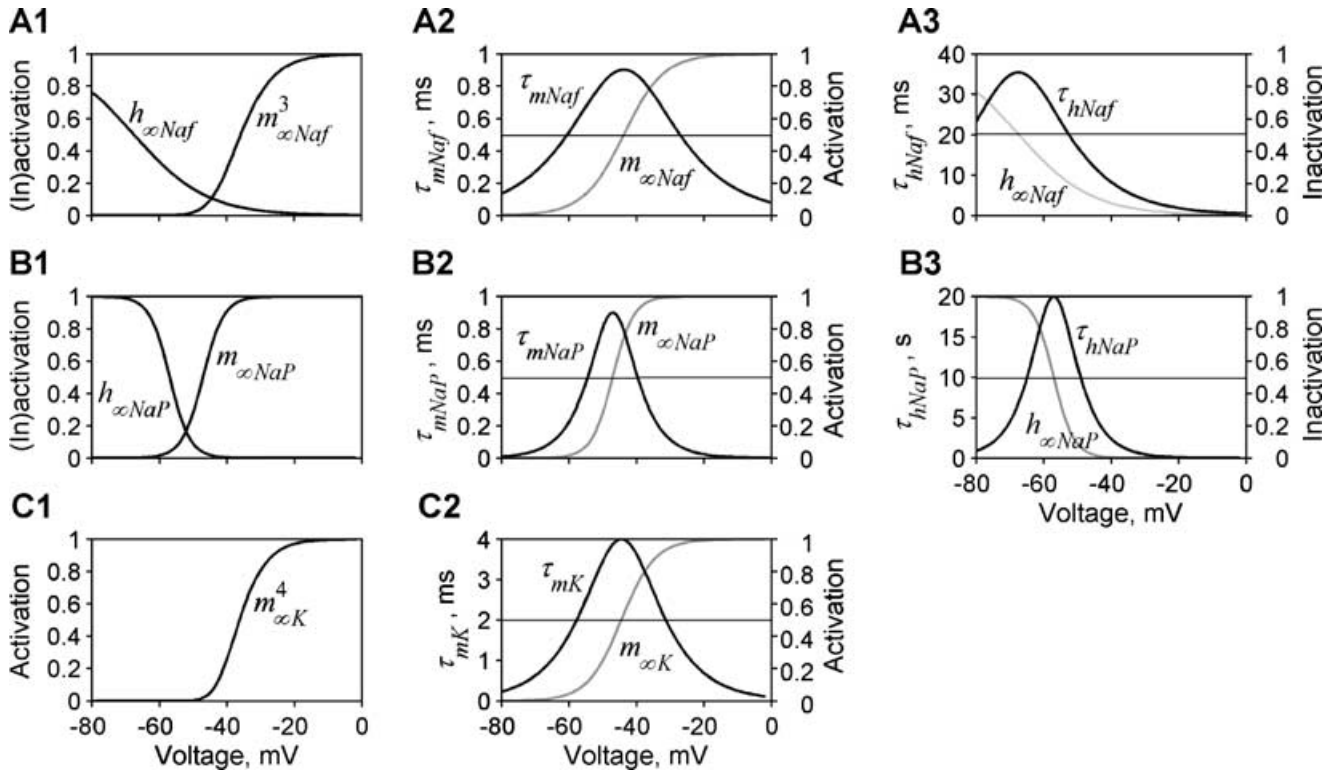

FIG. 1. Steady-state voltage-gating characteristics of the ionic channels in the model. (A1–A3) Fast sodium channel: steady-state activation and inactivation variables (A1) and time constant for activation (A2, bold line, left *y* axis) and inactivation (A3, bold line, left *y* axis). (B1–B3) Persistent sodium channel: steady-state activation and inactivation variables (B1) and time constant for activation (B2, bold line, left *y* axis) and inactivation (B3, bold line, left *y* axis). (C1 and C2) Delayed-rectified potassium channel: steady-state activation variable (C1) and time constant for activation (C2, bold line, left *y* axis).

bursts at any values of $[K^+]_o$ and input drive. A reduction of $\bar{g}_K$ below 25 nS made the mechanism for spike generation unstable; bursts could not be generated and were replaced by long-lasting plateau potentials.

Intracellular and extracellular concentrations of sodium and potassium (Table 1) were set to meet the average data for neurons in the mammalian nervous system (Johnson & We, 1997). The reversal potentials for sodium and potassium currents were calculated on the basis of the Nernst equation 6. The leakage reversal potential was calculated using the Goldman equation 7. The excitatory synaptic reversal potential was set to zero ($E_{synE} = 0$ mV). The value of the whole-cell capacitance, $C = 36.2$ pF, was set on the basis of experimental measurements of the membrane capacitance in neurons dissociated from the rostral ventrolateral medulla of the rat (Kawai *et al*., 1999). The value of the whole-cell capacitance used in the model was consistent with the recent data obtained by Del Negro *et al*. (2002a) for pBC pacemaker neurons (32 ± 3 pF). The leakage conductance $g_{leak} = 2$ nS was set to fit the experimentally measured minimal cell input resistance $R_{in} = 500$ MΩ (see Mazza *et al*., 2000). This value was consistent with the value of $R_{in} = 430 \pm 56$ MΩ which was experimentally estimated for the pBC pacemaker neurons by Del Negro *et al*. (2002a).

The heterogeneity of neurons within the population was set by a random distribution of maximal conductances for the persistent sodium, delayed-rectified and leakage channels ($\bar{g}_{NaP}$, $\bar{g}_K$, g_{leak}), values of external excitatory drive to each neuron (g_{Edr}) and weights of synaptic interconnections (w_{ij}) (see mean values ±SD in Table 1). These parameters were chosen for random distribution because they (or their relationships) explicitly defined the excitability of neurons within the population and the mode of their firing activity (tonic or bursting). In each simulation, the values of these parameters were randomly assigned from normal distributions. The following SDs were assigned (see Table 1): 10% of basic mean values for $\bar{g}_{NaP}$, $\bar{g}_K$ and w_{ij}, 30% for g_{leak} and 20% for g_{Edr}. These SDs restrained the randomized parameters within the physiological range. A higher value of SD for g_{leak} was assigned to reproduce some level of background asynchronous population activity as was observed in experimental recording of pBC activity. Similar to the earlier simulations of Butera *et al*. (1999b) and Del Negro *et al*. (2001), we did not randomize the maximal conductance of the fast sodium channel as changes in this conductance caused no alteration in the mode of neuronal firing behaviour. The particular values of randomized parameters were assigned during the phase of initialization which preceded the phase of actual simulation. To assign changes in a randomized parameter during simulation, we multiplied the value of this parameter in each neuron by the corresponding coefficient without a re-initialization of model parameters. For all simulations, initial conditions were chosen randomly from a uniform distribution across the physiological range for each variable, and a setting period of 60 s was allowed in each simulation before data were collected. Each simulation was repeated 20–30 times, and demonstrated qualitatively similar behaviour at the chosen SD of the parameters.

Computer simulation

All simulations were performed on a Pentium IV computer, 1.7 GHz/512 MB (Dell) with a Windows 2000 operating system using (i) a special simulation package *NeuroSim* (developed at Drexel University by I. A. Rybak, S. N. Markin, D. G. Ivashko and N. A. Shevtsova using Microsoft Visual C ++) and (ii) *MATLAB* 6.0 (MathWorks, Inc.) Differential equations were solved using the exponential Euler integration method (MacGregor, 1987) with a step of 0.1 ms in *NeuroSim*, and a variable-order integration method based on the numerical differentiation formulas, NDFs, in ode15s routine for solution of

differential equations in MATLAB. Differences in results of simulations using the above two methods were $<10^{-4}$ for each variable.

Experimental procedures

Rhythmic slice preparation

Spontaneous rhythmic transverse slices were obtained from neonatal rats (P0–P4), which were deeply anaesthetized with ether and then decapitated. The brainstem was rapidly removed in artificial cerebrospinal fluid (aCSF) continuously oxygenated with carbogen (5% CO_2, 95% O_2; pH 7.4). The brainstem was then glued against a cube of agar which was fixed on a plexiglas plate. The mounted brainstem was positioned in a vibroslicer (Leica VT1000E) and cut serially in the caudal direction. Slices were cut 300–500 μm caudal to the anterior inferior cerebellar arteries and were of 700 μm thickness. Once cut, the slice was put in a recording chamber with the rostral surface up and closest to the surface of the bath. Slices were pinned down on a silicone ring placed in the middle of the aCSF stream. Slices used in experiments displayed some typical anatomical landmarks including XII nucleus and XII axon tract, inferior olive, pyramidal tract and NTS (as previously described, e.g. by Ramirez *et al*., 1996). These anatomical landmarks were used for the initial localization of the pre-Bötzinger region. The preparation of slices took no more than 10 min. During each experiment, the brainstem slice was continuously bathed with equilibrated aCSF at a rate of 15 mL/min at a temperature of 27.5–28 °C. All procedures described are in accordance with the guidelines for care and use of laboratory animals adopted by the European Community, law 86/609/EEC.

Recording procedures

We recorded population activity from the pre-Bötzinger region. In 2/3 of slices, population activity of the pBC was recorded simultaneously with the activity of XII nerve rootlet. In all these experiments, integrated activity from the pBC was synchronous with integrated XII activity. This provided evidence that the hypoglossal output motor activity followed (and was driven by) the activity of the pBC neural population.

Both pBC and XII recordings were performed with suction electrodes which had an inner diameter of 100–150 μm and a resistance of 110–185 kΩ when filled and measured in aCSF. Recordings began immediately after positioning the slice in the recording chamber. Neural activities were allowed to stabilize in terms of amplitude and frequency before experiments started (30–45 min). Raw activities of the XII rootlets and of the pre-Bötzinger region were filtered (1–3 kHz and 300Hz), amplified (10^5 times) and integrated ($\tau = 100$–200 ms). Raw and integrated signals were continuously recorded through a CED 1401 interface (Spike3 acquisition program, CED, Cambridge, UK) connected to a personal computer.

Application of drugs

4-aminopyridine (4-AP) and tetraethylammonium-chloride (TEA) are commonly used as specific blockers of voltage-gated potassium currents. 4-AP is usually applied in concentrations of 40–2000 μM (e.g. Huguenard & Prince, 1991; McCormick, 1991; Del Negro & Chandler, 1997; Martina *et al*., 1998), and TEA is commonly used in concentrations of 1–10 mM (Huguenard & Prince, 1991; McCormick, 1991; Martina *et al*., 1998; Kang *et al*., 2000; Martin-Caraballo & Greer, 2000).

Sodium cyanide (NaCN) was used in a separate series of experiments. This drug is known to cause histotoxic hypoxia thereby mimicking severe hypoxia *in vivo* (Solomon, 2002; Solomon *et al*., 2000; 1 mM) and anoxia in isolated *in vitro* brainstem preparations (Völker *et al*., 1995, 2–5 mM) or in neurons cultured from the rostral ventrolateral medulla (Mazza *et al*., 2000, 0.5–10 mM). NaCN is also known as an activator of the persistent sodium channels (Hammarström & Gage, 2000, 5 mM; Kawai *et al*. 1999, 1 mM).

Riluzole was used in a third series of experiments to block persistent sodium currents (Urbani & Belluzzi, 2000). This drug was previously used in the same preparation (Del Negro *et al*., 2002b, 1–200 μM; Koizumi & Smith, 2002, 5–30 μM; Parkis *et al*. 2002, 20 μM).

All drugs were obtained from Sigma Inc. (France). Stock solutions of 4-AP, TEA and NaCN were prepared in saline. Riluzole was prepared in 50% HCl 0.1 N (final HCl solution was 0.2%). All drugs were diluted to final concentrations in aCSF in a reservoir which was continuously oxygenated with carbogen. Fluid from this reservoir was applied to the slice through a tap connected to the main inflow line. 4-AP was applied in concentrations of 50–200 μM, TEA in concentrations of 2 or 4 mM, NaCN in concentration of 2 mM and riluzole in concentrations of 25 and 50 μM. Washout of drugs was performed by passing fresh aCSF-3 (aCSF containing 3 mM of potassium; see below) through the recording chamber.

Experimental protocols

Experiments were started with aCSF containing (in mM): NaCl, 126; KCl, 5; $NaHCO_3$, 21; NaH_2PO_4, 0.5; $MgSO_4$, 1; $CaCl_2$, 1.5; glucose, 30; equilibrated with carbogen (CO_2 5%, O_2 95%, pH 7.4, 27.5–28 °C). This aCSF is designated throughout the text as aCSF-5 (i.e. aCSF solution containing 5 mM of potassium). We first used aCSF-5 to ensure that the slice could generate rhythmic activity. Any slice that had no rhythmic activity with aCSF-5 was rejected and was not used in further experiments. Once recordings were stabilized, we replaced the aCSF-5 with one containing 7 mM of potassium (aCSF-7). With aCSF-7, all slices generated stable rhythmic activity. Then we replaced aCSF-7 with the aCSF containing 3 mM of potassium (aCSF-3) which was considered an aCSF corresponding to the normal *in vivo* conditions. The effects of potassium current blockers (4-AP, TEA) and of NaCN were examined with aCSF-3 after rhythmic activities were completely abolished. The effect of riluzole was tested using the rhythmically active slices superfused with aCSF-7.

Analysis of rhythmic activities

Off-line analysis consisted of measuring both amplitude and frequency of integrated activities recorded from the pBC and XII nerve. The number of cycles analysed depended on the effects observed. Frequencies of bursting activities were averaged within relevant groups and presented as mean ±SD. For each group, the average amplitude of bursting activities triggered by application of 4-AP, TEA or NaCN in presence of aCSF-3 was analysed using the average amplitude of bursting activity in the same group at aCSF-7 as a reference.

Results

Results of computational modelling

Modelling single pBC pacemaker neuron

Our single-neuron model was developed on the basis of the model of Butera *et al*. (1999a). This model had been developed before the sodium currents were characterized in pBC and, hence, was based on generic descriptions of channel kinetics. In the present study, we incorporated data derived explicitly from experimental characterization of sodium channels in pBC neurons (Shevtsova *et al*., 2002; Rybak *et al*., 2003).

Similar to the model of Butera *et al*. (1999a), our model demonstrated the ability of a single pBC pacemaker neuron to generate tonic or rhythmic bursting activities depending on conditions (Fig. 2). As described in detail by Butera *et al*. (1999a), the burst generating

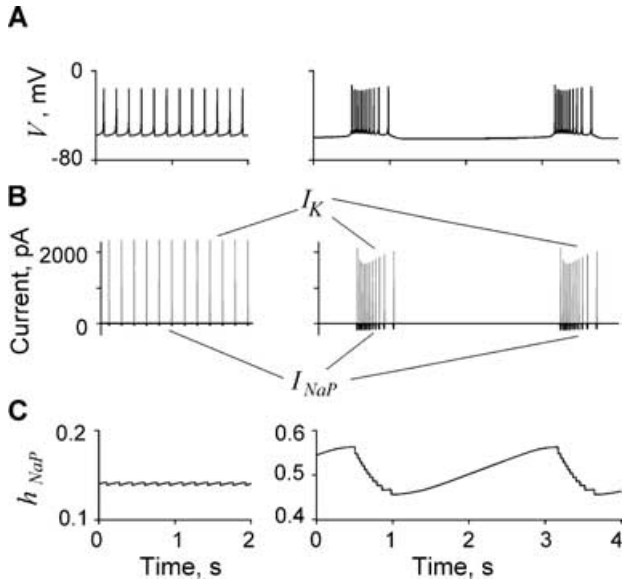

FIG. 2. Example of firing behaviour of the model of single pacemaker neuron in the tonic (left column) and bursting (right column) modes. Bursting was triggered by elevation of $[K^+]_o$ from 3 to 9 mM. (A) Temporal dynamics of neuronal membrane potential. (B) Ionic currents: I_K (grey) and I_{NaP} (black). (C) Dynamics of the persistent sodium inactivation variable (h_{NaP}). Note that the amplitude of the delayed-rectifier current (I_K) is lower in the bursting mode than in the tonic mode, whereas the amplitude of the persistent sodium current (I_{NaP}) and the ratio of I_{NaP}/I_K are much higher in the bursting mode.

mechanism in this neuron type is explicitly dependent on the slow voltage-dependent inactivation of the persistent sodium current (h_{NaP}). h_{NaP} slowly increases during the interburst intervals and decreases during burst periods (Fig. 2C). Comparison of amplitudes of the persistent sodium (I_{NaP}) and delayed-rectifier (I_K) currents in the bursting mode vs. the tonic activity mode demonstrated that I_K amplitude was smaller, whereas I_{NaP} amplitude and the ratio I_{NaP}/I_K were higher in the bursting mode (Fig. 2B).

Firing behaviour of neurons in the model was dependent on the maximal conductances for I_{NaP} and I_K, as well as on the extracellular potassium concentration ($[K^+]_o$) and the excitatory tonic drive to the neuron (g_{Edr}). Figure 3A shows that an increase in $[K^+]_o$ to exceed some threshold (7.9 mM) triggered endogenous bursting activity. Further increase in $[K^+]_o$ produced an increase in burst frequency and a decrease in burst duration and then, at a higher level of $[K^+]_o$, bursting activity switched to tonic firing. In contrast, an increase in g_{Edr} at a normal level of $[K^+]_o$ (3 mM) did not produce bursting, but increased the frequency of tonic activity (Fig. 3B). At a higher level of $[K^+]_o$ (e.g. at $[K^+]_o = 7.5$ mM; see Fig. 3C), bursting activity was triggered when g_{Edr} exceeded some threshold. Then, the frequency of bursts increased with an increase in g_{Edr} until the neuron switched to tonic firing at a higher level of g_{Edr} (Fig. 3C).

Computational investigation of the model has shown that bursting behaviour of a single neuron exists in a small area of parameter space. Specifically, Fig. 4 shows three areas corresponding to different modes of single-cell activity as a function of g_{Edr} and $[K^+]_o$, and the dependence of these areas upon I_{NaP} and I_K. As seen in this figure, endogenous bursting in the model could not be triggered at the $[K^+]_o = 3$ mM (see also Fig. 3B), but only at an increased value of $[K^+]_o$ with a certain level of cellular excitability (g_{Edr}). Our analysis has shown that firing behaviour of the model is strongly dependent on the relationships between the I_{NaP}, I_K and the leakage current (I_{leak}). The role of the ratio between the I_{NaP} and the voltage-independent I_{leak} currents for endogenous bursting activity in the pBC has been investigated earlier (e.g. Del Negro *et al*., 2001; Koshiya *et al*., 2001; Del Negro *et al*., 2002a). In contrast, the role of voltage-gated potassium currents (such as the delayed-rectifier) and their relationships with I_{NaP} in the generation of endogenous bursting activity have not been considered.

In each plot in Fig. 4, three separate areas represent three different modes of single-neuron firing behaviour: 'silence', 'bursting', and 'tonic activity'. These areas are separated by two borderlines, one of which defines the threshold of neuron firing ('threshold borderline') and the other separates 'bursting' from 'tonic activity' ('bursting borderline'). Figure 4A–C shows the changes in the position of these borderlines resulting from the changes in the maximal conductance of the persistent sodium ($\bar{g}_{NaP}$) and delayed-rectifier potassium ($\bar{g}_K$) channels. The position of the threshold borderline is controlled by $\bar{g}_{NaP}$ (and g_{leak}, not shown) and is almost independent on $\bar{g}_K$ (Fig. 4A–C). An increase in $\bar{g}_{NaP}$ shifts this borderline towards lower values of g_{Edr} and $[K^+]_o$ and, hence, widens the bursting area. The position of the bursting borderline is mostly controlled by $\bar{g}_K$ (and g_{leak}, not shown) and is almost independent of $\bar{g}_{NaP}$ (Fig. 4A–C). A decrease in $\bar{g}_K$ shifts this borderline toward higher values of g_{Edr} and $[K^+]_o$ and also widens the bursting area. A decrease in $\bar{g}_{NaP}$ produces the opposite effect, a reduction in the bursting area (Fig. 4A–C). An increase in $\bar{g}_{NaP}$ allows bursting activity at a wider range of $[K^+]_o$ (at fixed values of $\bar{g}_K$ and g_{Edr}), which is consistent with Butera *et al*. (1999a) and Del Negro *et al*. (2001). In contrast, an increase in $\bar{g}_K$ reduces the range of $[K^+]_o$ allowing bursting activity (at fixed values of $\bar{g}_{NaP}$ and g_{Edr}). Hence, we have concluded that I_K and I_{NaP} may control switching between different modes of single-neuron firing behaviour.

Another important conclusion from the above analysis is that an increase in excitatory drive to the neuron and an increase in $[K^+]_o$ produce different effects on the neuronal firing behaviour. Specifically, an increase in g_{Edr} at the normal level of $[K^+]_o$ depolarizes the cell without changing the balance between I_{NaP} and I_K. Relatively large I_K provides a deep membrane repolarization after each generated spike. This repolarization hyperpolarizes the membrane below the level of I_{NaP} activation and, hence, prohibits endogenous bursting (see Fig. 2). In contrast, an increase in $[K^+]_o$ produces two simultaneous effects: one is the cellular depolarization (via shifting the leakage reversal potential E_{leak} to more positive values; see equation 7), the other is the suppression of I_K by shifting the reversal potential for potassium E_K to more positive values (see equations 6 and 2). Therefore at higher levels of $[K^+]_o$ the reduced I_K cannot produce the necessary afterspike repolarization and, hence, cannot restrain the endogenous I_{NaP}-dependent bursting activity (see Fig. 2B).

Our finding that the borderlines between different functional modes in single-neuron firing behaviour are dependent upon $[K^+]_o$ and channel conductances $\bar{g}_K$ and $\bar{g}_{NaP}$ (Fig. 4A–C) leads to the conclusion that bursting behaviour of the single neuron may be triggered from the silent state by either an increase in $[K^+]_o$ (Fig. 5A) or an augmentation of $\bar{g}_{NaP}$ (Fig. 5C). At the same time, the neuronal firing behaviour may be switched from tonic firing to endogenous bursting by a suppression of $\bar{g}_K$ (Fig. 5B).

Modelling a population of pBC pacemaker neurons with mutual excitatory connections

To investigate firing behaviour of a population of pacemaker neurons, we modelled a population of 50 neurons with all-to-all excitatory synaptic connections similar to the models by Butera *et al*. (1999b) and Del Negro *et al*. (2001). To incorporate heterogeneity in neurons within the population, some parameters of neurons ($\bar{g}_{NaP}$, $\bar{g}_K$ and g_{leak}) and neuronal connections (g_{Edr} and w_{ij}) were assigned from

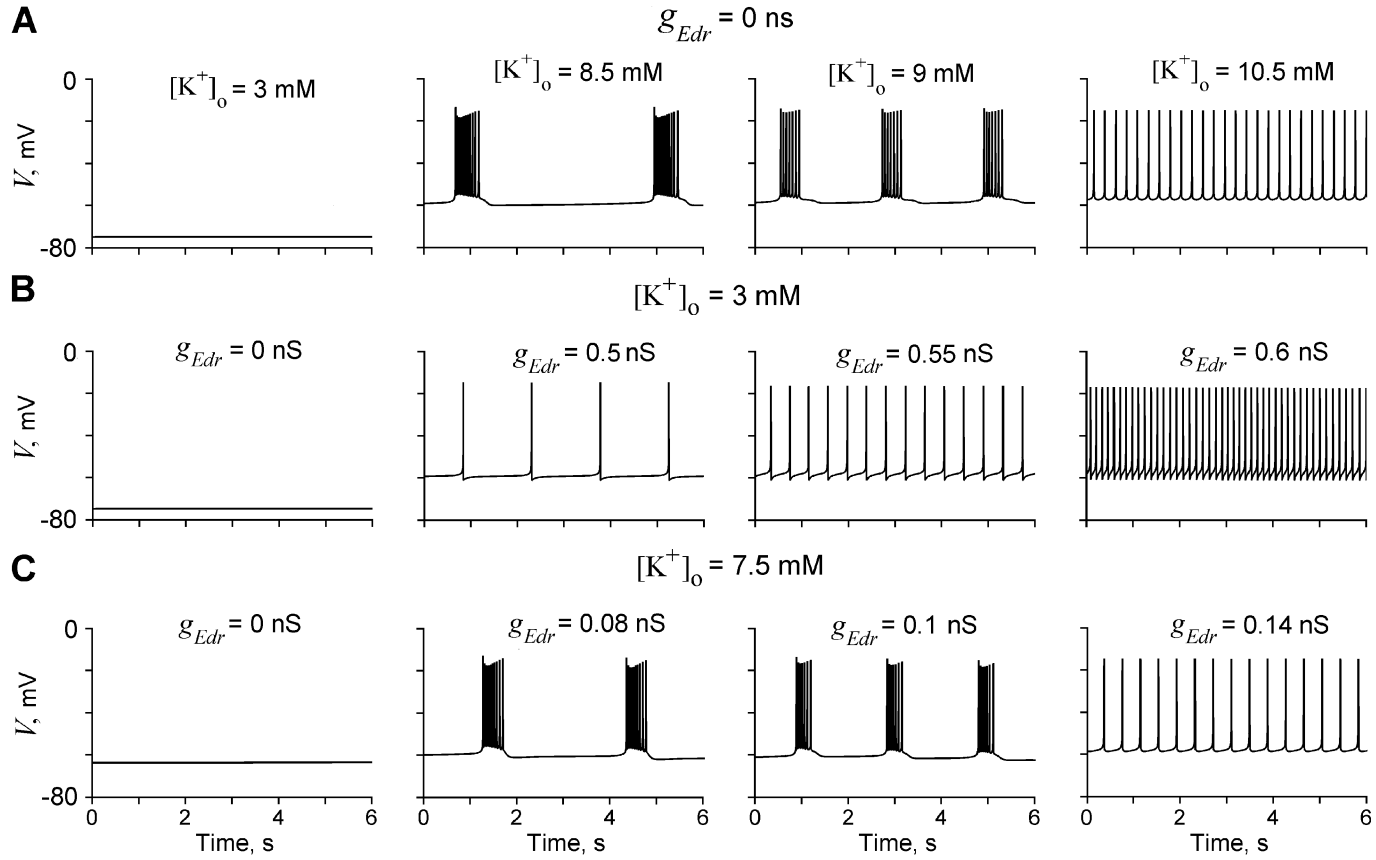

FIG. 3. Firing activity of the model of a pBC pacemaker neuron under different conditions. (A) Firing behaviour of the model without excitatory drive ($g_{Edr} = 0$) at different levels of $[K^+]_o$. Value of $[K^+]_o$ is shown above each trace and increases from left to right. An increase in $[K^+]_o$ triggers the rhythmic bursting activity at some threshold of $[K^+]_o$. Further increases in $[K^+]_o$ produce an increase in burst frequency and a decrease in burst duration. At a higher level of $[K^+]_o$, bursting switches to tonic firing. (B) Firing behaviour of the model at $[K^+]_o = 3$ mM. Value of g_{Edr} is shown above each trace and increases from left to right. An increase in g_{Edr} causes an increase in the frequency of tonic activity. Note the absence of bursting activity at any value of g_{Edr}. (C) Firing behaviour of the model at $[K^+]_o = 7.5$ mM; g_{Edr} increases from left to right. Bursting activity is triggered when g_{Edr} exceeds some threshold. The frequency of bursts increases with an increase in g_{Edr} until the neuron switches to tonic firing at a higher level of g_{Edr}.

normal distribution (see Table 1). Some parameters and mathematical descriptions used in our model differed from those in the models of Butera *et al*. (1999b) and Del Negro *et al*. (2001). For example, we incorporated data on sodium current kinetics derived from the direct experimental measurements in pBC neurons (Shevtsova *et al*., 2002; Rybak *et al*., 2003). However, the behaviour of our model was qualitatively similar to that of the previous models and our simulations confirmed most major conclusions and predictions of the models by Butera *et al*. (1999b) and Del Negro *et al*. (2001). At the same time, we focused on the investigation of the specific roles of the potassium-rectifier and persistent sodium channels in the triggering or suppression of endogenous bursting activity in the pBC. These roles were not considered in the previous models.

Our simulations have shown that both the excitatory synaptic interconnections between neurons and the randomization of neuronal parameters within the population make the area of parameters for population bursting much wider than that for a single pacemaker neuron (see also Butera *et al*., 1999b and Del Negro *et al*., 2001). Figure 6 shows an example of our simulations at the population level. An increase in $[K^+]_o$ to exceed some threshold (5.6 ± 0.6 mM; variation is dependent on the initial randomization of parameters) triggered bursting activity in the population. Further increase in $[K^+]_o$ produced an increase in the burst frequency and a desynchronization of neuronal activity, which in turn caused a decrease in the burst amplitude and an increase in asynchronous background activity. At a higher level of $[K^+]_o$, the population bursting activity switched to a high-level asynchronous firing (Fig. 6A).

An increase in the g_{Edr} at the normal level of $[K^+]_o$ (3 mM) did not produce bursting in the population but increased the level of asynchronous activity (Fig. 6B).

At higher values of $[K^+]_o$ (e.g. at $[K^+]_o = 5$ mM; see Fig. 6C), population bursting was triggered when g_{Edr} exceeded some threshold (0.04 ± 0.006 nS). The frequency of bursts increased with an increase in g_{Edr}. However, increasing g_{Edr} produced a desynchronization of neuronal activities which in turn decreased the amplitude of population bursts and increased the level of asynchronous activity. Finally, at some level of g_{Edr} the firing behaviour of the population switched to a high-level asynchronous firing (Fig. 6C).

Figure 7 shows an example of our simulations of the population bursting activity induced by the augmentation of $[K^+]_o$ (Fig. 7A), and changes of $\bar{g}_K$ (Fig. 7B) and $\bar{g}_{NaP}$ (Fig. 7C) at the basic level of $[K^+]_o$ (3 mM). In Fig. 7A, $[K^+]_o$ was increased from the basic level to higher levels. Bursting was initiated when $[K^+]_o$ exceeded some threshold (e.g. 5.0 ± 0.4 mM at $g_{Edr} = 0.05$ nS) and terminated when $[K^+]_o$ returned to the basic level. An increase in the $[K^+]_o$ augmentation produced an increase in the frequency of population bursting, a decrease in the burst amplitude and an increase in the level of background asynchronous activity (Fig. 7A).

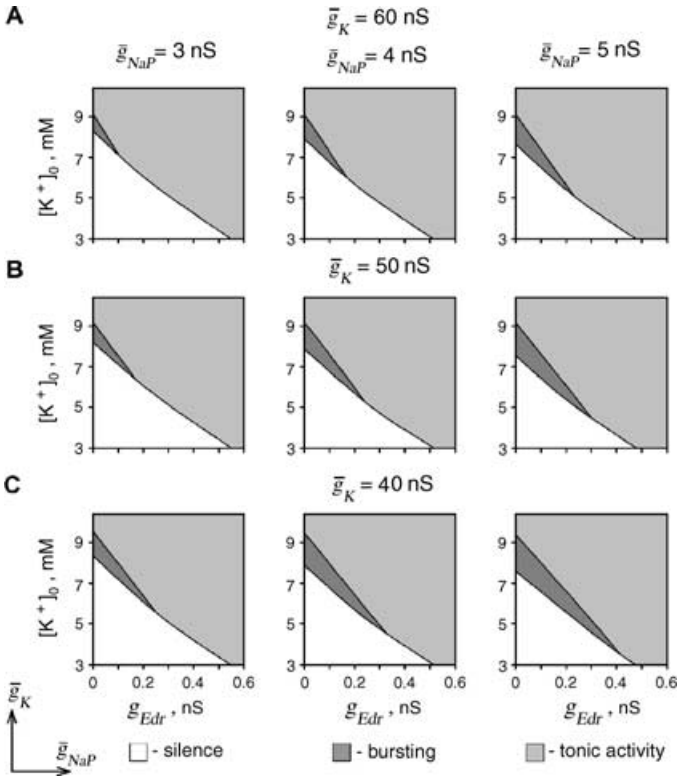

FIG. 4. 'Silence', 'bursting' and 'tonic activity' modes in single-cell firing behaviour as a function of g_{Edr} and $[K^+]_o$. The diagram in the centre of the figure corresponds the basic values of model parameters ($\bar{g}_{NaP} = 4.0$ nS; $\bar{g}_K = 50.0$ nS; $g_{leak} = 2.00$). Note the shifting of the borderlines between the areas corresponding to different modes with the changes in maximal conductances of the persistent sodium $\bar{g}_{NaP}$ (increases from left to right) and delayed-rectifier $\bar{g}_K$ (increases bottom up from C to A) channels.

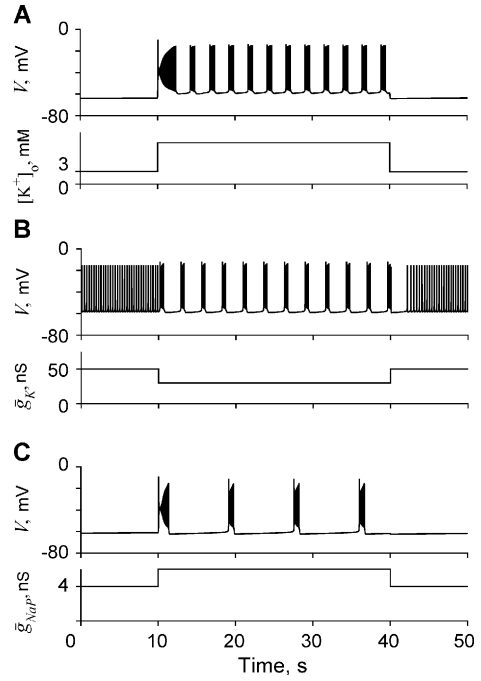

FIG. 5. Triggering endogenous bursting activity in the model of a single pacemaker neuron. (A) An example of triggering endogenous bursting activity by the elevation of $[K^+]_o$ (bottom trace; $[K^+]_o$ was increased from 3 to 7.5 mM). (B) An example of transition from tonic activity to bursting by reduction of $\bar{g}_K$ (bottom trace; $\bar{g}_K$ was reduced from 50 to 30 nS). (C) An example of triggering endogenous bursting activity by augmentation of $\bar{g}_{NaP}$ (bottom trace; $\bar{g}_{NaP}$ was increased from 4 to 6 nS).

Reduction of $\bar{g}_K$ (at $[K^+]_o = 3$ mM) from its basic level (50 nS) (by 31% at $g_{Edr} = 0.05$ nS) also produced a population bursting activity (Fig. 7B). Small clusters of synchronously discharging neurons emerged in the population. These clusters defined a low-amplitude population bursting. A larger reduction of $\bar{g}_K$ caused an emergence of larger synchronized clusters (up to synchronous discharges of the whole population) which produced a low-frequency–high-amplitude population bursting. This high-amplitude bursting could coexist with the high-frequency–low-amplitude bursting (Fig. 7B at $\bar{g}_K = 31$ nS and Fig. 8). Further reduction of $\bar{g}_K$ eliminated the low-amplitude bursting and produced an increase in the frequency of high-amplitude bursting with a reduction in burst amplitude and slight increase in background activity (Fig. 7B). The triggered bursting activity disappeared when $\bar{g}_K$ returned to the basic level of 50 nS.

Augmentation of $\bar{g}_{NaP}$ (at $[K^+]_o = 3$ mM) from the basic level, 4 nS, (by 50% at $g_{Edr} = 0.05$ nS) also caused population bursting (Fig. 7C). The population bursting induced by augmentation of $\bar{g}_{NaP}$ was similar to that produced by reduction of $\bar{g}_K$ described above. A moderate augmentation allowed the low-frequency–high-amplitude bursting to coexist with the high-frequency–low-amplitude bursting (Fig. 7C at $\bar{g}_{NaP} = 6.4$ nS). The $\bar{g}_{NaP}$-initiated bursting disappeared when $\bar{g}_{NaP}$ returned to the basic level of 4 nS.

Our simulation also demonstrated that, at moderate levels of reduction of $\bar{g}_K$ or augmentation of $\bar{g}_{NaP}$ and some degree of randomization of neuronal and network parameters, the population could simultaneously generate high-frequency–low-amplitude and low-frequency–high-amplitude bursting activities which were completely defined by synchronized clusters of neurons (subpopulations) emerging within the population (see Fig. 7B at $\bar{g}_K = 31$ nS, Fig. 7C at $\bar{g}_{NaP} = 6.4$ nS, and Fig. 8).

In summary, the major prediction from the above modelling studies was that rhythmic bursting activity in a population of pacemaker neurons in the pBC may be initiated by either (i) an increase in the extracellular potassium concentration, (ii) a suppression of the voltage-gated potassium-rectifier channels or (iii) by an augmentation of the persistent sodium channels.

Our *in vitro* studies described below have been performed with the primarily goal of testing our modelling predictions.

Results of in vitro *studies*

Effect of changes in extracellular potassium concentration

Thirty-six slices (13 with pBC recordings and 23 with both pBC and XII recordings) which generated rhythmic bursting activity with aCSF-5 were investigated. The bursting activity observed with aCSF-5 was less robust than that obtained when the solution was replaced with aCSF-7. The elevation of $[K^+]_o$ to 7 mM increased the level of synchronization within the pBC bursting neuronal population which resulted in an increase in the amplitude of bursts in both pBC and XII recordings.

With aCSF-7, all slices generated population bursting activity with a frequency ranging from 4 to 15 bursts/min and an average frequency of 9.64 ± 5.4 bursts/min [Figs 9, 10A–D, 11(A1 and B1), 12A and B, and 13(A1)]. In all slices with dual recordings ($n = 23$), integrated population activity in the pBC was in phase with integrated XII activity [e.g. see Figs 9, and 11(A1 and B1), 12A and B, and 13(A1)]. In four slices, in addition to the regular bursting activity one could observe additional

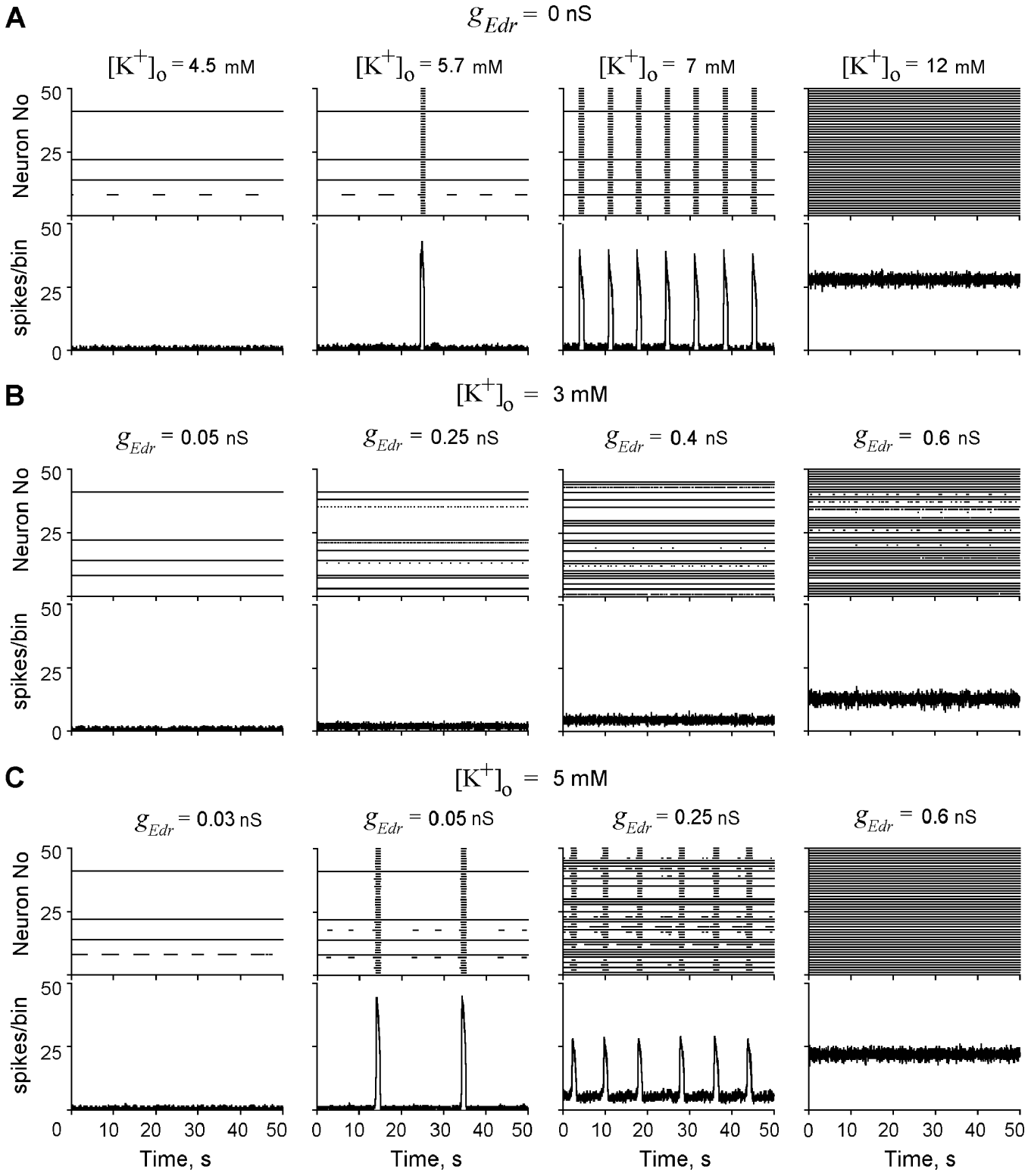

FIG. 6. Firing activity of the model of a population of pacemaker neurons under different conditions. The result of each simulation is represented by two diagrams: the top diagram is a raster plot for spike times in all 50 cells, sorted on the ordinate axis by cell index number; the bottom diagram is a corresponding integrated histogram of population activity (bin size = 10 ms). (A) An example of firing behaviour of the model without excitatory drive ($g_{Edr} = 0$) at different $[K^+]_o$. Values of $[K^+]_o$ are shown at the top. $[K^+]_o$ increases from left to right. An increase in $[K^+]_o$ triggers rhythmic bursting activity in the population at some threshold of $[K^+]_o$. Further increase in $[K^+]_o$ produces an increase in burst frequency, an increase in the level of background asynchronous activity and a decrease in burst amplitude. At a higher level of $[K^+]_o$, firing activity of the population switches to asynchronous firing. (B) An example of firing behaviour of the model at $[K^+]_o = 3$ mM. Mean value of g_{Edr} in the population is shown at the top and increases from left to right. An increase in g_{Edr} causes an increase in the level of asynchronous activity. Note the absence of bursting at any value of g_{Edr}. (C) An example of firing behaviour of the model at $[K^+]_o = 5$ mM; g_{Edr} increases from left to right. Bursting activity is triggered when g_{Edr} exceeds some threshold. Further increase in g_{Edr} produces an increase in burst frequency, an increase in the level of background asynchronous activity and a decrease in burst amplitude. At a higher level of g_{Edr}, firing activity of the population switches to asynchronous firing.

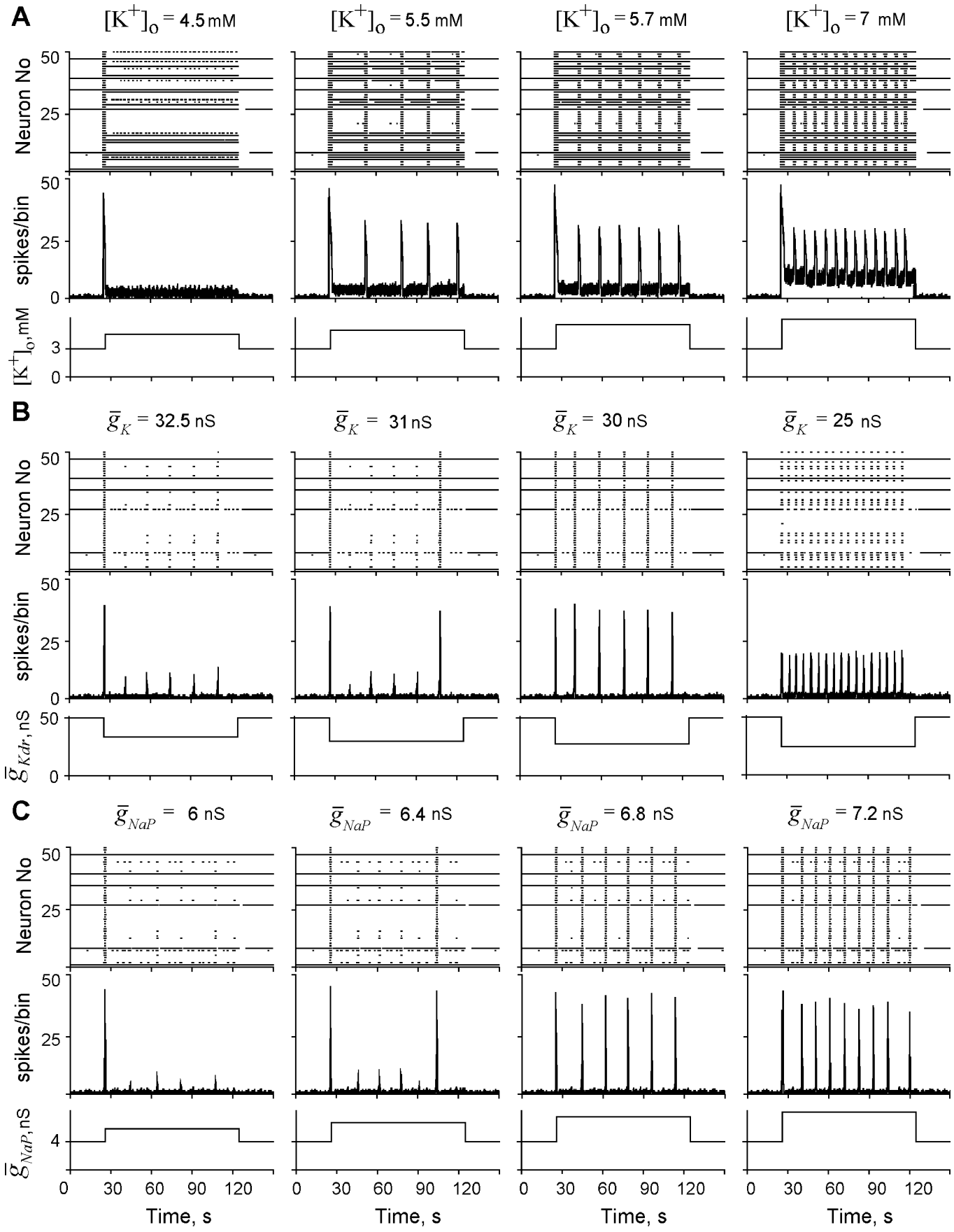
A
$[K^+]_o$ = 4.5 mM
$[K^+]_o$ = 5.5 mM
$[K^+]_o$ = 5.7 mM
$[K^+]_o$ = 7 mM
Neuron No
spikes/bin
$[K^+]_o$, mM
B
$\bar{g}_K$ = 32.5 nS
$\bar{g}_K$ = 31 nS
$\bar{g}_K$ = 30 nS
$\bar{g}_K$ = 25 nS
$\bar{g}_{Kdr}$, nS
C
$\bar{g}_{NaP}$ = 6 nS
$\bar{g}_{NaP}$ = 6.4 nS
$\bar{g}_{NaP}$ = 6.8 nS
$\bar{g}_{NaP}$ = 7.2 nS
$\bar{g}_{NaP}$, nS
Time, s

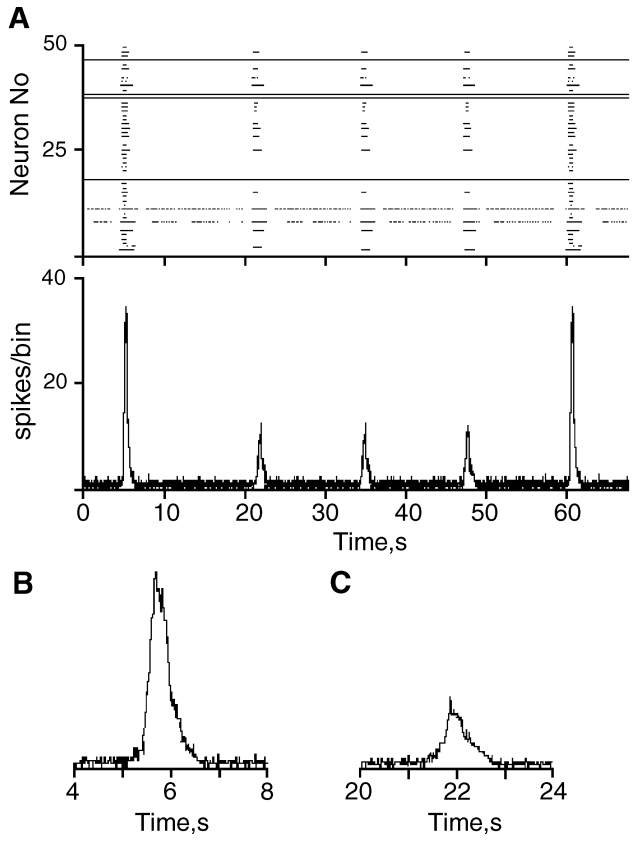

FIG. 8. An example of two simultaneous types of population bursting triggered by a reduction of $\bar{g}_K$. $\bar{g}_K$ was reduced from 50 to 31 nS at $[K^+]_o = 3$ mM. (A) The raster plot and integrated histogram of population activity. Note an extended delay of the first low-amplitude burst after the high-amplitude burst. (B,C) Examples of single bursts of (B) the low-frequency–high-amplitude bursting activity and of (C) the high-frequency–low-amplitude bursting activity.

low-frequency–high-amplitude bursts. These bursts were generated with a frequency ranging from 0.5 to 1.8 bursts/min and had average amplitude ≈28% higher than the average amplitude of regular bursts (see an example in Fig. 10D).

Reduction of $[K^+]_o$ to 3 mM (by switching to aCSF-3) stopped rhythmic activity in 29 of 30 slices tested (96.7%; e.g. see Figs 9 and 10A–D). The delay in cessation of rhythmic activity was between 1 and 35 min. The cessation of rhythmic activity in slices at $[K^+]_o = 3$ mM confirmed our modelling prediction that population activity in the pBC should not be present at the physiological level of $[K^+]_o$ (3 mM) (see Figs 6A and C, and 7A).

Effect of potassium channel blockers on slice activity at $[K^+]_o = 3$ mM

Our modelling studies predicted that population bursting activity in the pBC can be triggered at the normal physiological level of $[K^+]_o$ by a direct suppression of voltage-gated potassium currents. To test this prediction two potassium channels blockers, 4-AP and TEA, were applied on 23 of 29 slices (12 with solely pBC and 11 with dual recordings) whose rhythmic bursting activity was abolished by switching the solution to aCSF-3.

4-AP (50–200 μM) was applied in 15 experiments performed on 14 slices and triggered rhythmic bursting activity in all applications (100%; see examples with solely pBC recordings in Figs 10A and B and with dual recordings in Fig. 11, A2 and A3). The first phenomenon induced in pBC recordings was a deflection of the background activity level (Figs 10A and B, and 11, A2) on which triggered bursting was superimposed. In all slices with dual recordings, population activity in the pBC triggered by 4-AP was in phase with XII discharges (Fig. 11, A2 and A3).

Interestingly, the results of our experiments with 4-AP applications allowed us to distinguish two groups in all tested slices. In the first group ($n = 10$), 4-AP triggered low-frequency–high-amplitude bursting activities with a frequency range from 1.25 to 3.0 bursts/min and average frequency of 1.81 ± 0.7 bursts/min. The amplitude of generated bursts was similar to that observed with aCSF-7 (91.7% on average). Examples of such bursting activity triggered by 4-AP are shown in Figs 10A, and 11(A2 and A3).

In the second group ($n = 5$), application of 4-AP triggered high-frequency–low-amplitude bursting activities whose frequencies ranged from 9.5 to 30 bursts/min with average frequency of 21.6 ± 6.6 bursts/min and relatively small amplitude of bursts (on average, 52% of the burst amplitude observed with aCSF-7). An example of such bursting activity triggered by 4-AP is shown in Fig. 10B.

TEA (2 or 4 mM) was applied in 10 experiments performed on nine slices and triggered rhythmic bursting activities in eight applications (80%; see examples with pBC recordings in Figs 10C and D and with dual recordings in Fig. 11, B2 and B3). The initial deflection of the background activity observed in pBC recordings was less than that during 4-AP applications (see Figs 10C and D, and 11, B2). In all slices with dual recordings, population activity in the pBC triggered by TEA was in phase with XII nerve discharges (see Fig. 11, B2 and B3). The frequency of triggered bursts ranged from 1.0 to 8.0 bursts/min with mean frequency of 4.1 ± 2.7 bursts/min. The amplitude of bursts triggered by TEA was smaller than that measured with aCSF-7 (64% on average; see an example in Fig. 10C).

In four cases (two in the second group of slices with 4-AP application and two in slices with TEA application) the dominant high-frequency–low-amplitude bursting activity was superposed with additional bursts of higher amplitude and lower frequency (between 0.6 and 1.3 bursts/min) (see an example for TEA in Fig. 10, D1 and D2). In all such cases, the superposed bursting activities were initially present in the same slices perfused with aCSF-7 (see Fig. 10D). The low-frequency–high-amplitude bursting was similar to that observed in the first group of slices with applications of 4-AP (see above).

During washout of the drugs (4-AP or TEA), bursting activity in both pBC and XII rootlet ceased with a variable delay (30–60 min). The effect of each drug was repeatable on the same slice after wash out.

In summary, blocking potassium currents with 4-AP and TEA at $[K^+]_o = 3$ mM triggered bursting activity in 23 of 25 experiments (92%). Application of drugs triggered either a high-frequency–low-

FIG. 7. Triggering endogenous bursting activity in the model of the population of pacemaker neurons. (A) An example of triggering endogenous bursting activity by elevation of $[K^+]_o$ (bottom traces). $[K^+]_o$ is increased from 3 mM to higher levels. The augmentation of $[K^+]_o$ increases from left to right. An increase in $[K^+]_o$ augmentation increases the burst frequency and the level of background asynchronous activity and decreases the burst amplitude. (B) An example of triggering endogenous bursting activity by reduction of the mean value of $\bar{g}_K$ in the population. The mean value of $\bar{g}_K$ is reduced from 50 nS to lower values. The reduction increases from left to right. (C) An example of triggering endogenous bursting activity by augmentation of the mean value of $\bar{g}_{NaP}$ in the population. The mean value of $\bar{g}_{NaP}$ is increased from 4 nS to higher values. The augmentation increases from left to right. Note the triggering of two types of bursting in B and C, one with high-frequency–low-amplitude bursts and the other with low-frequency–high-amplitude bursts.

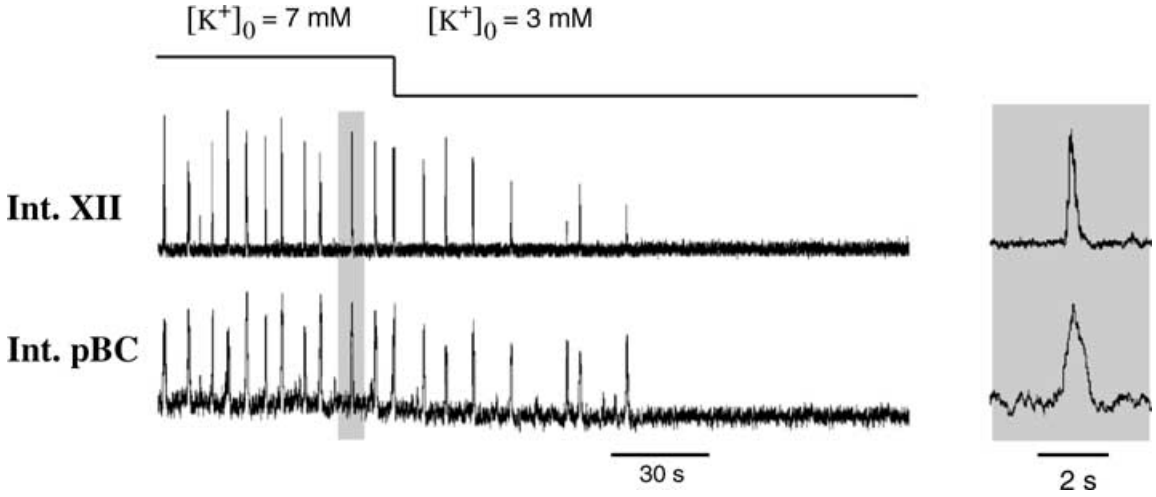

FIG. 9. Effect of changing extracellular potassium concentration on the discharges of XII nerve and population activity in the pBC. Reducing $[K^+]_o$ from 7 to 3 mM (shown at the top) stopped rhythmic activity in the slice. An example of single bursts generated at $[K^+]_o = 7$ mM is shown on the right on an expanded time scale.

amplitude bursting or a low-frequency–high-amplitude bursting. In several cases the two types of bursting coexisted in the same slice.

Effect of the persistent sodium channel blocker on rhythmic slices

The effects of riluzole on rhythmically active slices were studied to investigate the role of persistent sodium currents in the generation of endogenous rhythmic activity in pBC. Riluzole is known as a specific blocker of the persistent sodium current (Urbani & Belluzzi, 2000).

Riluzole (25 or 50 μM) was applied in six experiments on six slices which generated rhythmic bursting activity with aCSF-7 while recording solely pBC population activity (two slices) or both pBC and XII nerve activities (four slices). Riluzole abolished rhythmic activity in five of six slices (83.3%). Once abolished, rhythmic activity did not recover within 15–60 min washout.

In three slices, riluzole completely abolished rhythmic activity during drug application with variable delays (see an example in Fig. 12A). In two other slices, rhythmic activity was abolished after 6.1 and 8.0 min washout, respectively (see an example in Fig. 12B). In one slice, riluzole did not stop rhythmic activity after 10 min of application and rhythmic activity was still present after 15 min washout.

Triggering endogenous bursting activity with NaCN

NaCN was applied in the presence of aCSF-3 at a concentration of 2 mM in eight slices with simultaneous recordings of pBC and XII nerve. Applications of NaCN triggered phase-locked activities in the pBC and XII rootlet in all applications (100%). An example is shown in Fig. 13(A1–A3). Application of NaCN produced a biphasic change in the tonic level of activity and the frequency of triggered bursts stabilized in the second, falling, phase of the response (see Fig. 13, A2). The triggered frequency ranged from 2.5 to 9.5 bursts/min with average frequency of 6.2 ± 2.4 bursts/min. The amplitude of bursts triggered by NaCN was not significantly different from that observed with aCSF-7 (75% on average). Triggered activities slowly disappeared during washout of NaCN in about 30–40 min.

Discussion

Some limitations of the present modelling and experimental studies

The modelling studies described in this report had a number of limitations resulting mainly from a lack of particular data. Specifically, only one possible I_{NaP}-dependent pacemaker mechanism was considered, in which termination of the generated bursts was based on the slow inactivation of the persistent sodium channels. The kinetics of slow inactivation of the persistent sodium channels is a critical issue in this model type (e.g. see Butera *et al*., 1999a). However, these kinetics have not been experimentally characterized in pBC neurons and require further investigations. Other possible mechanisms for termination of the burst may be based, for example, on slowly activating potassium channels (e.g. see Butera *et al*., 1999a, Model 2; Rybak *et al*., 2001, 2002, Model 2) or on intracellular calcium accumulation followed by the activation of calcium-dependent potassium channels (e.g. Rybak *et al*., 2001, 2002, Model 3).

In the present model, the classical Nernst (equation 6) and Goldman (equation 7) equations were used to describe reversal potentials for potassium and leakage channels, respectively. However, it is currently unknown to what degree these classical equations are obeyed in pBC neurons with changing $[K^+]_o$. For example, Forsythe & Redman (1988) found a deviation of E_K values from those predicted by the Nernst equation at $[K^+]_o < 10$ mM. Alternatively, other investigators reported that changes in E_K followed the Nernst equation in a wide range of values of $[K^+]_o$ (e.g. see Huguenard *et al*., 1991; Xu & Adams, 1992; Cox *et al*., 1995; Pan *et al*., 1995; Jolas & Aghajanian, 1997; Bischoff *et al*., 1998).

Modelling neural populations in the present study was limited to simulation of only homogenous population with all-to-all connections. Specifically, all neurons in the simulated populations had the same repertoire of ionic channels, and sparse interconnections between neurons within the population were not considered.

Our modelling study has predicted that the normally expressed delayed-rectified potassium current may restrain the generation of endogenous I_{NaP}-dependent bursting activity in the pBC, and that a suppression of this current can trigger (release) this activity. Earlier, a similar prediction was made in respect of the transient potassium-A current (Rybak *et al*., 2001, 2002). Although the present model has considered only the delayed-rectifier potassium current, we suggest that our prediction concerns a wider series of voltage-gated potassium currents in pBC neurons. Unfortunately, voltage-gated potassium currents have so far not been experimentally characterized in the pBC. At the same time, a large number of different noninactivating (similar to the classical delayed-rectifier) as well as slowly and rapidly inactivating potassium currents (of the A-type) were found in the rodent central nervous sys-

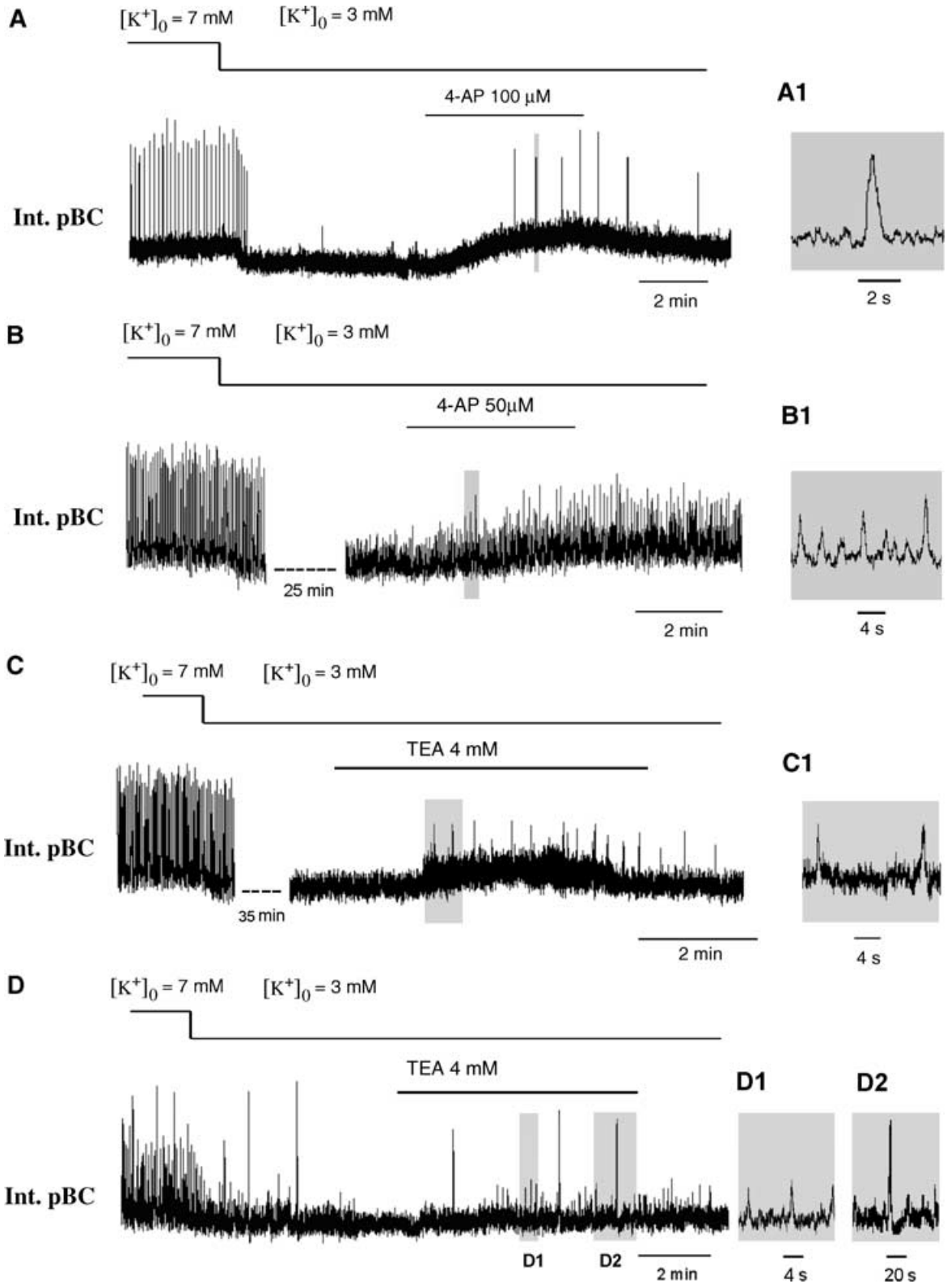

FIG. 10. Effects of changing extracellular potassium concentration $[K^+]_o$ from 7 to 3 mM and of subsequent application of potassium channel blockers (4-AP and TEA) on the integrated population activity in the pBC. In each experiment, reducing $[K^+]_o$ from 7 to 3 mM (shown at the top of each plot) stopped rhythmic activity in the pBC. (A) An example of low-frequency–high-amplitude bursting activity in the pBC triggered by the application of 4-AP (100 μM) at 3 mM $[K^+]_o$. A1 shows a single burst at an expanded time scale. (B) An example of high-frequency–low-amplitude bursting activity in the pBC triggered by the application of 4-AP (100 μM) at 3 mM $[K^+]_o$. B1 shows triggered activity at an expanded time scale. (C) An example of bursting activity triggered in the pBC by the application of TEA (4 mM) at 3 mM $[K^+]_o$. C1 shows triggered activity at an expanded time scale. (D) An example of simultaneous high-frequency–low-amplitude and low-frequency–high-amplitude activities in the pBC triggered by the application of TEA (4 mM) at 3 mM $[K^+]_o$. D1 and D2 show, respectively, high-frequency–low-amplitude and low-frequency–high-amplitude bursts on an expanded time scale.

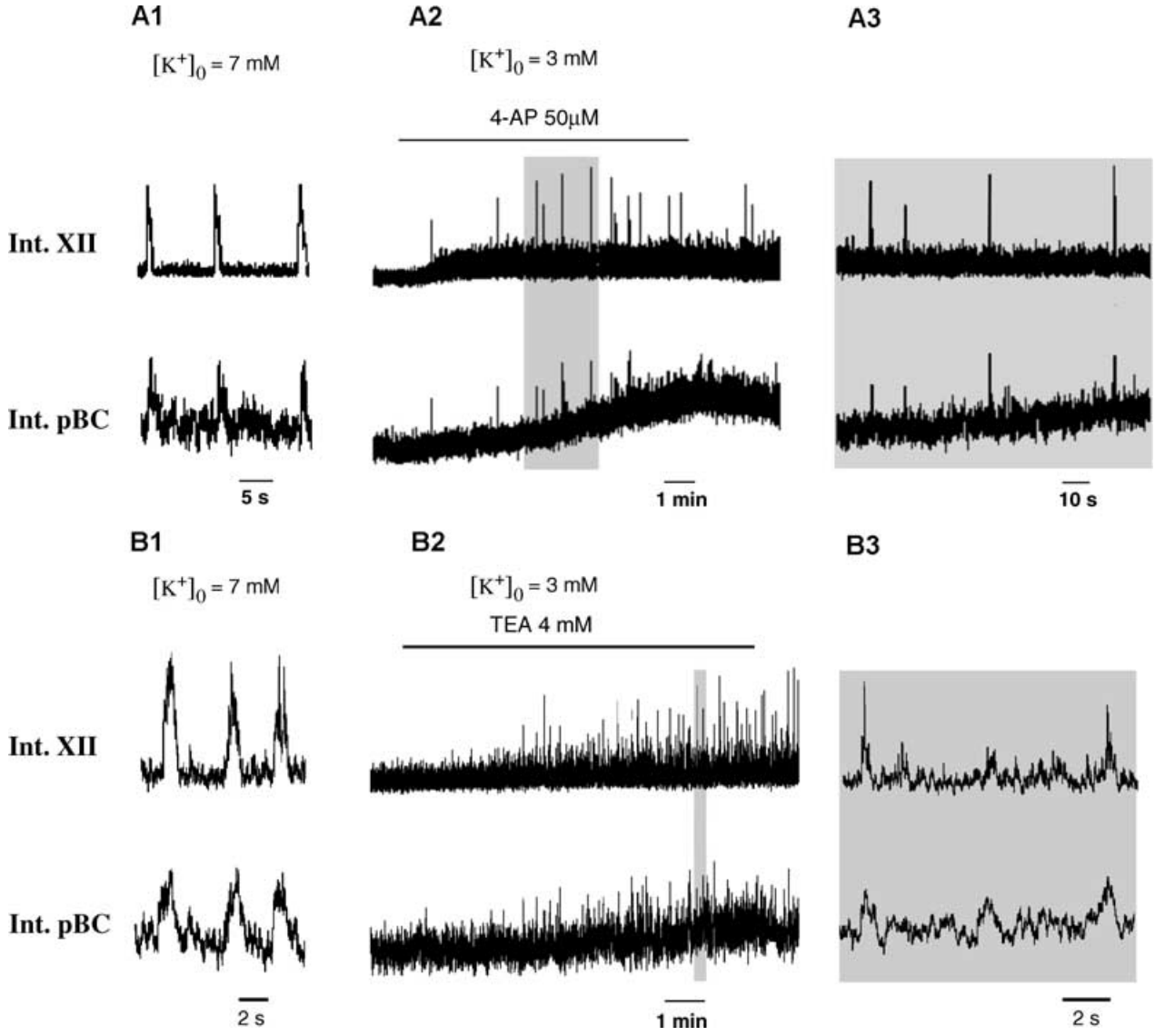

FIG. 11. Triggering endogenous bursting activity by the application of 4-AP (A1–A3) and TEA (B1–B3) on slices with simultaneous recording of XII rootlet and integrated population activity in the pBC. (A1 and B1) Activity in the slices at $[K^+]_o = 7$ mM. (A2 and B2) Triggering of endogenous bursting activity in the slices (nonrhythmic at $[K^+]_o = 3$ mM) by applications of 4-AP or TEA. (A3,B3) Triggered activities in the slices at expanded time scales.

tem. (Huguenard & Prince, 1991; McCormick, 1991; Kirsch & Drewe, 1993; Del Negro & Chandler, 1997; Martina *et al*., 1998; Lape & Nistri, 1999; Kang *et al*., 2000; Martin-Caraballo & Greer, 2000; Etzion & Grossman, 2001). These potassium currents have different sensitivities to TEA and 4-AP. In general, TEA is known to inhibit noninactivating potassium currents of the delayed-rectifier type, whereas 4-AP is less specific and inhibits both noninactivating and inactivating (A-type) potassium currents with generally a greater inhibition of the latter. At the same time, Etzion & Grossman (2001) demonstrated that 4-AP strongly inhibited the delayed-rectifier channels in cerebellar Purkinje cells. As we noted above, the exact types of potassium channels in pBC neurons and their voltage-dependent kinetics are currently unknown. Similar to neurons from other regions of the rat central nervous system, these neurons should have a number of noninactivating (delayed-rectifier-like) and inactivating (e.g. A-like) voltage-gated potassium channels. In our experiments, we used both the above blockers and found that each of them could trigger endogenous bursting activity in the pBC. Voltage-independent (leak-type) potassium channels could be also attenuated by the blockers and, hence, could contribute to the generation of endogenous bursting activity, as analysed by Butera *et al*. (1999a,b) and Del Negro *et al*. (2001). This may rather concern 4-AP, because TEA does not normally influence ionic channels which are open at rest. For 4-AP, Etzion & Grossman (2001) found that this blocker did not influence resting membrane potential. However, generally, the effects of the two blockers on the leak-type potassium channels have not been systematically investigated.

Endogenous bursting activity in the pBC in vitro

The role of elevated $[K^+]_o$

The ability of the pBC to generate endogenous rhythmic bursting activity has been demonstrated *in vitro* in many studies. The important question is what conditions are necessary for stable generation of this intrinsic rhythm? A series of computational and experimental studies has demonstrated that endogenous neural oscillations may be induced by the elevation of extracellular potassium concentration $[K^+]_o$ (e.g.

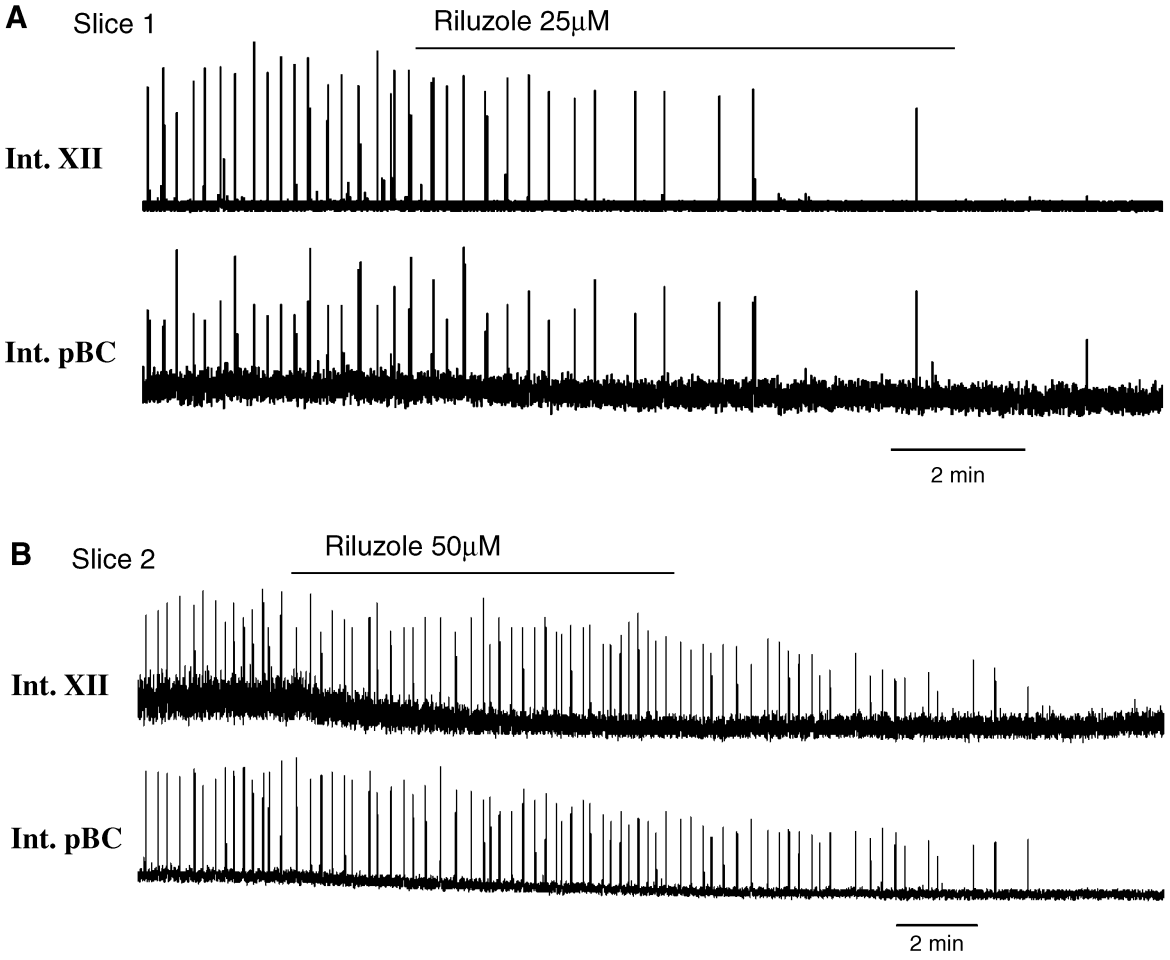

FIG. 12. Effects of riluzole on the endogenous bursting activity in the slice at $[K^+]_o = 7$ mM. (A) Riluzole (25 μM) abolished rhythmic activity in the slice during the application. (B) Riluzole (50 μM) abolished rhythmic activity in the slice after washout. Note that abolition of activity is gradual and starts with a decrease in the burst amplitude.

see Hahn & Durand, 2001; Marchetti *et al*., 2001). The analysis of publications in the area shows that in most cases the endogenous rhythmic activity in the pBC *in vitro* was triggered and maintained with the elevation of $[K^+]_o$ up to 7–9 mM (e.g. see Johnson *et al*., 1994; Shao & Feldman, 1997; Koshiya & Smith, 1999; Lieske *et al*., 2000; Thoby-Brisson & Ramirez, 2001; Del Negro *et al*., 2002b). Specifically, while visualizing the rhythmic activity in pBC with calcium-sensitive dye, Koshiya and Smith explicitly demonstrated that synchronized bursting activity was absent at low levels of $[K^+]_o$ but started at $[K^+]_o = 6$–9 mM (see fig. 2 in Koshiya & Smith, 1999). At the same time, the necessity of elevated $[K^+]_o$ for the stable generation and maintenance of endogenous rhythm in the pBC *in vitro* is still debated. For example, Del Negro *et al*. (2002b) stated that 'elevated $[K^+]_o$ is not required for bursting', with a reference to Del Negro *et al*. (2001). However, in that study the authors did increase $[K^+]_o$ to 9 mM (see Del Negro *et al*., 2002b, Methods), and in the referred paper the authors stated that 'rhythmic respiratory activity was maintained by raising the aCSF K^+ concentration to 5–8 mM' (see Methods in Del Negro *et al*., 2001). Johnson *et al*. (2001) studied isolated pBC 'islands' after a blockade of inhibition. $[K^+]_o$ was varied in the range of 3–15 mM. When inhibition was blocked, a stable bursting activity could occur at 4–5 mM of $[K^+]_o$, and the data shown in the paper (fig. 2B and C) demonstrate rhythmic activity starting from 5 mM of $[K^+]_o$. Pierrefiche *et al*., (2002) have also found that a concentration of $[K^+]_o = 5$ mM is the minimum required to maintain stable spontaneous rhythmic activity in the pBC.

Our previous modelling studies (Rybak *et al*., 2001, 2002) and the modelling results described in this report (see Figs 3, 4, 5A, 6 and 7A) suggest that elevation of $[K^+]_o$ is a critical condition for stable generation of endogenous rhythmic activity in the pBC *in vitro*. The present results of our *in vitro* studies provide strong support for this concept (see Figs 9A and 10A). In agreement with our simulations (e.g. Figs 6A and C, and 7A), all preparations used in our experimental studies demonstrated endogenous population rhythmic activity at $[K^+]_o \geq 5$ mM. However, as predicted by the model, reducing $[K^+]_o$ to the normal physiological level (3 mM) completely stopped endogenous bursting in 96.7% of preparations (Figs 9–11 and 13).

Our results are consistent with the data of Tryba *et al*. (2003), who recently studied the possibility of triggering the endogenous rhythm in the pBC *in vitro* at $[K^+]_o = 3$ mM. The authors intended to prove that rhythm in slices can be generated at the physiological level of $[K^+]_o$. While some pacemaker neurons continued to generate bursting activity (especially when inhibition was blocked), the population activity in pBC ceased in most preparations (40 of 52, 77%) when $[K^+]_o$ was lowered from 8 to 3 mM (Tryba *et al*., 2003). Our simulation also showed that, with substantial randomization of neuronal parameters, some neurons in the population could indeed generate endogenous

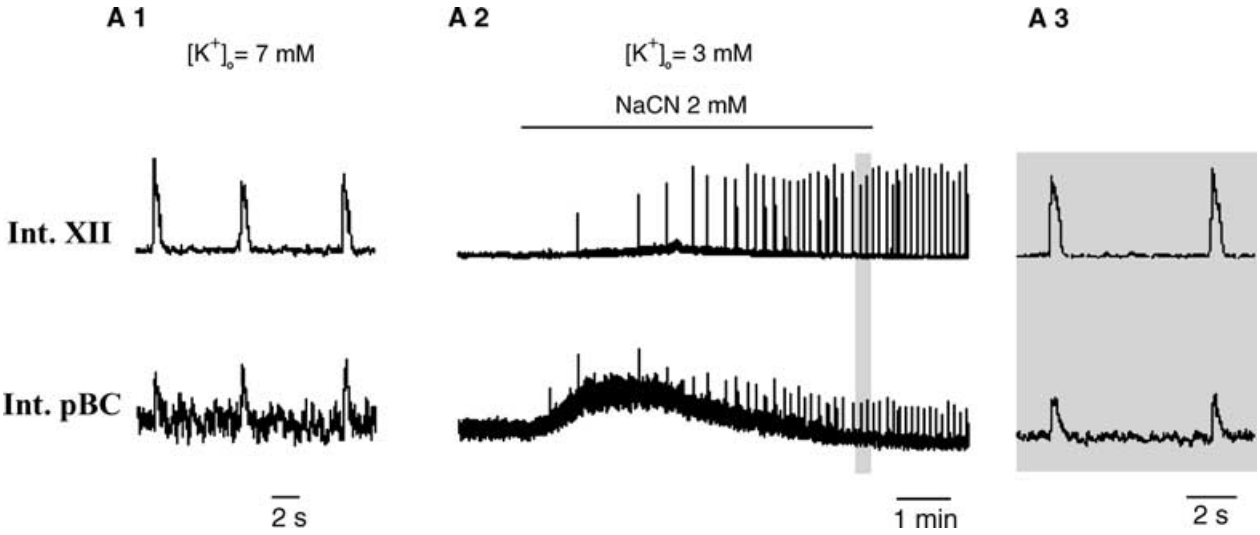

FIG. 13. Triggering endogenous bursting activity in the slice by the application of NaCN. (A1) Integrated XII and pBC population activities in the slice at $[K^+]_o = 7$ mM. (A2) Triggering of endogenous bursting activity in the slice at $[K^+]_o = 3$ mM by application of NaCN (2 mM). Note that triggered activity stabilized in the falling phase of background activity. (A3) Triggered bursting activity at an expanded time scale.

bursting activity at $[K^+]_o = 3$ mM, but the number of these neurons was not sufficient to synchronize and drive the whole population (our unpublished observation). Also, taking into account that most of propriobulbar neurons in the VRG are inhibitory, there is no reason to expect that inhibition within the pBC under normal conditions (e.g. *in vivo*) is reduced; this can rather occur during hypoxia.

The role of voltage-gated potassium currents

In the context of the above discussion, an interesting question is why does the elevation of $[K^+]_o$ induce endogenous bursting activity? The most common explanation is that pBC pacemaker neurons do not receive enough excitation *in vitro* and therefore the elevation of $[K^+]_o$ is necessary to increase the cellular excitability. However, as we show in the present modelling study, the effect of $[K^+]_o$ elevation on cellular behaviour differs from that of a direct increase in cellular excitability (e.g. by an increase in the excitatory drive to the neuron) (see Fig. 3A vs. B, plots in Fig. 4, and Fig. 6A vs. B). Specifically, an increase in excitatory drive only causes cellular depolarization whereas an increase in $[K^+]_o$ exerts two simultaneous effects: cellular depolarization (via the elevation of the leakage reversal potential) and a reduction of the voltage-gated potassium currents (I_K) through the change of the reversal potential for potassium. As a result, at higher levels of $[K^+]_o$ the reduced I_K cannot restrain endogenous I_{NaP}-dependent bursting activity.

We suggest that the reduction in I_K may indeed be a key mechanism for the release of endogenous bursting. In our computational study, we showed that bursting activity in both the model of the single pacemaker neuron (Fig. 6B) and the model of the neural population (Fig. 7B) may be induced at $[K^+]_o = 3$ mM by a suppression of the delayed-rectified potassium current. Moreover, the endogenous bursting in the population could be triggered from the same initial state by a suppression of I_K either via an increase in $[K^+]_o$ (Fig. 7A) or via a direct reduction of the channel conductance $\bar{g}_K$ (Fig. 7B).

These predictions of the model were confirmed in our *in vitro* studies. We showed that rhythmic bursting in medullary slices, non-rhythmic at $[K^+]_o = 3$ mM, could be triggered by the application of potassium current blockers (4-AP or TEA). In our experiments, 4-AP induced population bursting activity in the pBC (as well as in the XII rootlet in case of dual recordings) in 100% of applications (see Figs 10A and B, and 11, A2). TEA triggered population bursting in 80% of applications. All together, blockade of voltage-gated potassium channels at $[K^+]_o = 3$ mM triggered population bursting in the pBC and on XII output in 23 of 25 experiments (92%). This confirms the hypothesis that endogenous bursting in the pBC *in vitro* is critically dependent on the expression of voltage-gated potassium currents, and that the suppression of these currents, e.g. during hypoxia, may release endogenous rhythms in the pBC.

Interestingly, as in our simulations (see Figs 7 and 8), blocking potassium currents initiated two types of bursting activity: a low-frequency–high-amplitude type (first group of experiments with 4-AP application; see Figs 10A, and 11, A2 and A3) and a high-frequency–low-amplitude type (second group of experiments with 4-AP application and experiments with TEA application; see Figs 10B and C, and 11B). Moreover, similar to our model (Fig. 7B at $\bar{g}_K = 31$ nS, Fig. 7C at $\bar{g}_{NaP} = 6.4$ nS, and Fig. 8) and the model of Butera *et al.* (1999b), these two bursting types could coexist in the same preparation (e.g. Fig. 10D).

In this connection, Lieske *et al.* (2000) previously described three different bursting patterns generated in the pBC *in vitro* under different conditions, which the authors called 'eupnea', 'sighs' and 'gasps'. Specifically, the low-frequency–high-amplitude sighs could be recorded simultaneously with the high-frequency–low-amplitude eupnea. Similar to our simulations (Fig. 8) and experimental recordings (e.g. Fig. 10, D2), the low-frequency–high-amplitude bursts in the recordings of Lieske *et al.* (2000) ('sighs') produced a short depression or an extended delay of the next burst. Also, all three patterns were observed at a high concentration of $[K^+]_o$ (8 mM), which should significantly suppress potassium currents. 'Gasps' were seen in the falling phase of background activity under the anoxia conditions similar to that in our recordings after application of NaCN (Fig. 13, A2 and A3). It is tempting to speculate that different types of bursting activities in our modelling and experimental studies correspond to these described by Lieske *et al.* (2000). However, in our recordings we found no differences in burst shape between the high-amplitude and the low-amplitude bursts [either in simulation, e.g. Fig. 8B vs. C, or in our experimental recordings, e.g. Fig. 10 (A1 and D2 vs. B1, C1 and

D1)], neither did we find obvious differences in shape between the bursts triggered by the elevation of $[K^+]_o$ (e.g. Figs 9, 11, A1 and B1, and 13, A1) and those triggered by potassium channel blockers [e.g. Fig. 10 (A1, B1, C1, D1 and D2)] or NaCN (e.g. Fig. 13, A3). Based on our modelling studies, we suggest that all types of bursting in the pBC obtained in our *in vitro* studies occurred because of the same mechanism: suppression of potassium currents and release of I_{NaP}–dependent endogenous pacemaker activity. We also suggest that, similar to that in our simulations, the high-frequency–low-amplitude and low-frequency–high-amplitude bursting activities recorded in our experiments reflect different synchronized clusters of neurons emerging in a qualitatively uniform pacemaker population in the pBC under different conditions, and do not represent morphologically or functionally distinct neuronal networks.

The role of the persistent sodium current

It has been shown that the persistent sodium current (I_{NaP}) essentially contributes to the generation of intrinsic pacemaker activity in many types of neurons (e.g. see Llinàs *et al*., 1991; Dickson *et al*., 1997; Pennartz *et al*., 1997; Takakusaki & Kitai, 1997; Pape & Driesang, 1998; Bevan & Wilson, 1999). Smith and colleagues have suggested that I_{NaP} plays a major role in activation of pBC pacemaker neurons *in vitro* (Butera *et al*., 1999a,b; Smith *et al*., 2000; Del Negro *et al*., 2001). They also developed a series of computational models of single pacemaker neurons and populations of these neurons which closely reproduced the endogenous oscillations in the pBC (Butera *et al*., 1999a,b; Smith *et al*., 2000; Del Negro *et al*., 2001). Our models described herein used these models as a basis but incorporated data from experimental characterization of sodium channels in pBC (Shevtsova *et al*., 2002; Rybak *et al*., 2003). We believe that our modelling results provide additional support for the theoretical concept that a voltage-dependent, persistent-sodium-based mechanism is indeed essential for generation of endogenous neural oscillations in the pBC *in vitro*.

Our modelling results have also suggested that at the physiologically normal level of $[K^+]_o$ the I_{NaP}-dependent intrinsic neural oscillations in the pBC are restrained by voltage-gated potassium currents (see Fig. 2). Hence these oscillations may be triggered at $[K^+]_o = 3$ mM by either a suppression of the I_K (Figs 5B and 7B) or an augmentation of I_{NaP} (Figs 5C and 7C). Correspondingly, the suppression of I_{NaP} should eliminate endogenous oscillations.

To test this suggestion, we studied the effect of I_{NaP} blocker riluzole on endogenous rhythmic activity in pBC. In our experiments, application of riluzole abolished rhythmic bursting in five of six tested preparations (Fig. 12), which confirmed our prediction. These results, however, do not support recent data of Del Negro *et al*. (2002b), who reported that rhythmic activities of medullary slice preparations persisted after pharmacological blockade of the I_{NaP} by riluzole. Several investigations have recently reported that riluzole does block I_{NaP}-dependent rhythmic activity in pBC *in vitro* (Koizumi & Smith, 2002; Parkis *et al*., 2002). Our experimental results are consistent with this data. Further experimental studies are necessary to resolve this issue.

Endogenous bursting activity in the pBC and generation of the respiratory rhythm

Although the ability of the pBC to generate endogenous rhythmic bursting activity *in vitro* has been demonstrated in many studies, the role of these pacemaker-driven oscillations in the generation of the eupnoeic respiratory rhythm and its possible involvement in the generation of other patterns of breathing, such as gasping, is the subject of debate. The important issue is that the neuronal bursts recorded *in vitro* (as seen in both the hypoglossal nerve activity and the population activity from the pBC area) usually have a 'decrementing' pattern in which the spike frequency within the burst rapidly reaches a maximum and then slowly decrements. This pattern differs from the 'augmenting' pattern of the phrenic discharges recorded *in vivo* during eupnoea but is similar to gasping (Remmers, 1998; St-John, 1996; 1998; St-John & Paton, 2000). In addition, similar to the *in vitro* rhythm, gasping is resistant to a blockade of inhibitory transmission, and hence it has been suggested that gasping is also generated by a pacemaker-driven mechanism (St-John & Paton, 2002; St-John *et al*., 2002).

At the same time, some investigators believe that pacemaker neurons in the pBC comprise a 'kernel' for respiratory rhythm generation (Smith, 1997; Rekling & Feldman, 1998; Butera *et al*., 1999a,b; Smith *et al*., 2000; Del Negro *et al*., 2001; Gray *et al*., 2001). In frames of the 'kernel concept', Smith *et al*. (2000) recently suggested that both eupnoeic and gasping inspiratory patterns may originate from the pBC and represent different activity states. In contrast, other researchers suggest that the pacemaker-driven activity in the pBC is not expressed during eupnoea but plays a fundamental role in the generation of gasping (Fukuda, 2000; St-John, 1996; 1998; St-John *et al*., 2002). According to the 'switching concept' (Rybak *et al*., 2001, 2002; St-John *et al*., 2002), the pBC is considered a region explicitly responsible for switching from eupnoea generated by a network mechanism distributed in the pontomedullary region to gasping driven by pacemaker-based oscillations in the pBC.

Recent *in vivo* studies in the cat have demonstrated that the pBC may serve as a 'central hypoxia chemosensor'. Its activation by microinjection of DL-homocysteic acid (DLH) or sodium cyanide (NaCN producing local hypoxia in the pBC) elicits a 'rapid series of high-amplitude, rapid rate of rise, short-duration inspiratory bursts which are indistinguishable from gasps produced by severe systemic hypoxia' (Solomon *et al*., 2000; Solomon, 2002). Our present results show that NaCN may induce endogenous bursting *in vitro* (see Fig. 13), which is consistent with the above *in vivo* data.

The decrementing high-amplitude, short-duration discharges recorded from the phrenic nerve during gasping have a shape similar to that of the endogenous discharges recorded from *in vitro* preparations. Therefore, hypoxia may indeed produce a switch in the respiratory rhythm generation from a network mechanism for eupnoea to a pacemaker-driven mechanism for gasping (as suggested by Rybak *et al*., 2001, 2002; St-John *et al*., 2002). In support of this concept, it should be noted that hypoxia causes (i) a suppression of voltage-gated potassium currents, I_K (Jiang & Haddad, 1994; Conforti & Millhorn, 1997; Thompson & Nurse, 1998; Gebhardt & Heinemann, 1999; Liu *et al*., 1999; Lopez-Barneo *et al*., 2001) (ii) an augmentation of the persistent sodium current, I_{NaP} (Hammarström & Gage, 1998, 2000, 2002; Kawai *et al*., 1999; Horn & Waldrop, 2000), and (iii) an increase in external potassium concentration $[K^+]_o$ (Melton *et al.*, 1996), which produces an additional suppression of I_K.

In the present study, by combining *in vitro* experiments and computational modelling, we have shown that each of the above factors accompanying hypoxia may trigger endogenous bursting activity in the pBC. These results support the concept that gasping *in vivo* is driven by a pacemaker mechanism situated in the pBC. A recent study of the neurogenesis of gasping *in situ* (St-John *et al*., 2002) provided additional experimental evidence for this concept. Specifically, application of 4-AP and strychnine (to block glycine receptor mediated inhibition) in combination with an increase in $[K^+]_o$ converted the eupnoeic pattern of phrenic nerve discharge to a decrementing discharge similar to that recorded *in vitro* and during ischemia-induced gasping *in situ* (St-John *et al*., 2002).

Acknowledgements

I.A.R. was supported by NSF (0091942), NIH (NS046062-02 and HL072415-01) and ONR (N000140010719) grants. J.F.R.P. was supported by The British Heart Foundation (BS/93003). W.M.St-J. was supported by NIH (HL26091) and a Fogarty grant. The authors would like to thank Ms. F. Dussaussoy for technical assistance during *in vitro* experiments.

Abbreviations

4-AP, 4-aminopyridine; aCSF, artificial cerebrospinal fluid; aCSF-3, -5, -7, aCSF solution containing 3, 5 or 7 mM of potassium; *C*, whole-cell capacitance; *E*, reversal potential; *F*, Faraday constant; *g*, conductance; *h*, inactivation; *I*, current; K, delayed-rectifier potassium; *k*, slope factor; leak, leakage; *m*, activation; Naf, fast sodium; NaP, persistent sodium; pBC, pre-Bötzinger complex; *R*, universal gas constant; R_{in}, cell input resistance; *T*, temperature in degrees Kelvin; τ, time constant; TEA, tetraethylammonium chloride; *V*, voltage; w_{ij}, weights of synaptic interconnections.

References

Baker, M.D. & Bostock, H. (1998) Inactivation of macroscopic late Na^+ current and characteristics of unitary late currents in sensory neurons. *J. Neurophysiol.*, **80**, 2538–2549.

Bevan, M.D. & Wilson, C.J. (1999) Mechanisms underlying spontaneous oscillation and rhythmic firing in rat subthalamic neurons. *J. Neurosci.*, **19**, 7617–7628.

Bischoff, U., Vogel, W. & Safronov, B.V. (1998) Na^+-activated K^+ channels in small dorsal root ganglion neurones of rat. *J. Physiol. (Lond.)*, **510**, 743–754.

Butera, R.J., Rinzel, J.R. & Smith, J.C. (1999a) Models of respiratory rhythm generation in the pre-Bötzinger complex. I. Bursting pacemaker neurons. *J. Neurophysiol.*, **82**, 382–397.

Butera, R.J., Rinzel, J.R. & Smith, J.C. (1999b) Models of respiratory rhythm generation in the pre-Bötzinger complex. II. Populations of coupled pacemaker neurons. *J. Neurophysiol.*, **82**, 398–415.

Conforti, L. & Millhorn, D.E. (1997) Selective inhibition of a slow–inactivating voltage-dependent K^+ channels in rat PC12 cells by hypoxia. *J. Physiol. (Lond.)*, **502**, 293–305.

Cox, C.L., Huguenard, J.R. & Prince, D.A. (1995) Cholecystokinin depolarizes rat thalamic reticular neurons by suppressing a K^+ conductance. *J. Neurophysiol.*, **74**, 990–1000.

Del Negro, C.A. & Chandler, S.H. (1997) Physiological and theoretical analysis of K^+ currents controlling discharge in neonatal rat mesencephalic trigeminal neurons. *J. Neurophysiol.*, **77**, 537–553.

Del Negro, C.A., Johnson, S.M., Butera, R.J. & Smith, J.C. (2001) Models of respiratory rhythm generation in the pre-Bötzinger complex. III. Experimental tests of model predictions. *J. Neurophysiol.*, **86**, 59–74.

Del Negro, C.A., Koshiya, N., Butera, R.J. & Smith, J.C. (2002a) Persistent sodium current, membrane properties and bursting behavior of pre-Bötzinger complex inspiratory neurons *in vitro*. *J. Neurophysiol.*, **88**, 2242–2250.

Del Negro, C.A., Morgado-Valle, C. & Feldman, J.L. (2002b) Respiratory rhythm: an emergent network property? *Neuron*, **34**, 821–830.

Dickson, C.T., Mena, A.R. & Alonso, A. (1997) Electroresponsiveness of medial entorhinal cortex layer III neurons *in vitro*. *Neuroscience*, **81**, 937–950.

Etzion, Y. & Grossman, Y. (2001) Highly 4-aminopyridine-sensitive delayed rectifier current modulates the excitability of guinea pig cerebellar Purkinje cells. *Exp. Brain Res.*, **139**, 419–425.

Feldman, J.L. & Smith, J.C. (1989) Cellular mechanisms underlying modulation of breathing pattern in mammals. *Ann. NY Acad. Sci.*, **563**, 114–130.

Fleidervish, I.A., Friedman, A. & Gutnick, M.J. (1996) Slow inactivation of Na^+ current and slow cumulative spike adaptation in mouse and guinea-pig neocortical neurones in slices. *J. Physiol. (Lond.)*, **493**, 83–97.

Fleidervish, I.A. & Gutnick, M.J. (1996) Kinetics of slow inactivation of persistent sodium current in layer V neurons of mouse neocortical slices. *J. Neurophysiol.*, **76**, 2125–2130.

Forsythe, I.D. & Redman, S.J. (1988) The dependence of motoneurone membrane potential on extracellular ion concentrations studied in isolated rat spinal cord. *J. Physiol. (Lond.)*, **404**, 83–99.

Fukuda, Y. (2000) Respiratory neural activity responses to chemical stimuli in newborn rats: reversible transition from normal to 'secondary' rhythm during asphyxia and its implication for 'respiratory like' activity in isolated medullary preparation. *Neurosci. Res.*, **38**, 407–417.

Gebhardt, C. & Heinemann, U. (1999) Anoxic decrease in potassium outward currents of hippocampal cultured neurons in absence and presence of dithionite. *Brain Res.*, **837**, 270–276.

Gray, P.A., Janczewski, W.A., Mellen, N., McCrimmon, D.R. & Feldman, J.A. (2001) Normal breathing requires pre-Bötzinger complex neurokinin-1 receptor-expressing neurons. *Nature Neurosci.*, **4**, 927–930.

Hahn, P.J., Durand, D. & M. (2001) Bistability dynamics in simulations of neural activity in high-extracellular-potassium conditions. *J. Comput. Neurosci.*, **11**, 5–18.

Hammarström, A.K. & Gage, P.W. (1998) Inhibition of oxidative metabolism increases persistent sodium current in rat CA1 hippocampal neurons. *J. Physiol. (Lond.)*, **510**, 735–741.

Hammarström, A.K. & Gage, P.W. (2000) Oxygen-sensing persistent sodium channels in rat hippocampus. *J. Physiol. (Lond.)*, **529**, 107–118.

Hammarström, A.K. & Gage, P.W. (2002) Hypoxia and persistent sodium current. *Eur. Biophys. J.*, **31**, 323–330.

Horn, E.M. & Waldrop, T.G. (2000) Hypoxic augmentation of fast–inactivating and persistent sodium currents in rat caudal hypothalamic neurons. *J. Neurophysiol.*, **84**, 2572–2581.

Huguenard, J.R., Coulter, D.A. & Prince, D.A. (1991) A fast transient potassium current in thalamic relay neurons: kinetics of activation and inactivation. *J. Neurophysiol.*, **66**, 1304–1315.

Huguenard, J.R. & Prince, D.A. (1991) Slow inactivation of a TEA-sensitive K current in acutely isolated rat thalamic relay neurons. *J. Neurophysiol.*, **66**, 1316–1328.

Jiang, C. & Haddad, G.G. (1994) A direct mechanism for sensing low oxygen levels by central neurons. *Proc. Natl Acad. Sci. USA*, **91**, 7198–7201.

Johnson, S.M., Koshiya, N. & Smith, J.C. (2001) Isolation of the kernel for respiratory rhythm generation in a novel preparation: the pre-Bötzinger complex 'island'. *J. Neurophysiol.*, **85**, 1772–1776.

Johnson, S.M., Smith, J.C., Funk, G.D. & Feldman, J.L. (1994) Pacemaker behavior of respiratory neurons in medullary slices from neonatal rat. *J. Neurophysiol.*, **72**, 2598–2608.

Johnson, D. & We, S.M.-S. (1997) *Foundations of Cellular Neurophysiology.* The MIT Press, Cambridge, MA.

Jolas, T. & Aghajanian, G.K. (1997) Opioids suppress spontaneous and NMDA-induced inhibitory postsynaptic currents in the dorsal raphe nucleus of the rat *in vitro*. *Brain Res.*, **755**, 229–245.

Kang, J., Huguenard, J.R. & Prince, D.A. (2000) Voltage-gated potassium channels activated during action potentials in layer V neocortical pyramidal neurons. *J. Neurophysiol.*, **83**, 70–80.

Kawai, Y., Qi, J., Comer, A.H., Gibbons, H., Win, J. & Lipski, J. (1999) Effects of cyanide and hypoxia on membrane currents in neurons acutely dissociated from the rostral ventrolateral medulla of the rat. *Brain Res.*, **830**, 246–257.

Kirsch, G.E. & Drewe, J.A. (1993) Gating-dependent mechanism of 4-aminopyridine block in two related potassium channels. *J. Gen. Physiol.*, **102**, 797–816.

Koizumi, H. & Smith, J.C. (2002) Perturbation of respiratory pattern and rhythm *in vitro* by block of persistent sodium current (INaP). *Program No. 173.6 2002 Abstracts Viewer/Itinerary Planner* CD ROM. Society for Neuroscience, Washington, DC.

Koshiya, N., Del Negro, C., Butera, R.J. & Smith, J.C. (2001) Persistent sodium current (INaP) in pre-Bötzinger complex (pre-BötC) inspiratory neurons. *Program No. 243.3 2001 Abstracts Viewer/Itinerary Planner,* CD ROM. Society for Neuroscience, Washington, DC.

Koshiya, N. & Smith, J.C. (1999) Neuronal pacemaker for breathing visualized *in vitro*. *Nature*, **400**, 360–363.

Lape, R. & Nistri, A. (1999) Voltage-activated K^+ currents of hypoglossal motoneurons in a brain stem slice preparation from the neonatal rat. *J. Neurophysiol.*, **81**, 140–148.

Lieske, S.P., Thoby-Brisson, M., Telgkamp, P. & Ramirez, J.M. (2000) Reconfiguration of the neural network controlling multiple breathing patterns: eupnea, sighs and gasps. *Nature Neurosci.*, **3**, 600–607.

Liu, H., Moczydlowski, E. & Haddad, G.G. (1999) O_2 deprivation inhibits Ca^{2+}-activated K^+ channels via cytosolic factors in mice neocortical neurons. *J. Clin. Invest.*, **104**, 577–588.

Llinàs, R.R., Grace, A.A. & Yarom, Y. (1991) In vitro neurons in mammalian cortical layer 4 exhibit intrinsic oscillatory activity in the 10- to 50-Hz frequency range. *Proc. Natl Acad. Sci. USA*, **88**, 897–901.

Lopez-Barneo, J., Pardal, R. & Ortega-Saenz, P. (2001) Cellular mechanisms of oxygen sensing. *Annu. Rev. Physiol.*, **63**, 259–287.

MacGregor, R.I. (1987) *Neural and Brain Modeling*. Academic Press, New York.

Magistretti, J. & Alonso, A. (1999) Biophysical properties and slow voltage-dependent inactivation of a sustained sodium current in entorhinal cortex

layer-II principal neurons: a whole-cell and single-channel study. *J. Gen. Physiol.*, **114**, 491–509.
Marchetti, C., Beato, M. & Nistri, A. (2001) Evidence for increased extracellular [K^+] as an important mechanism for dorsal root induced alternating rhythmic activity in the neonatal rat spinal cord *in vitro*. *Neurosci. Lett.*, **304**, 77–80.
Martina, M., Schultz, J.H., Ehmke, H., Monyer, H. & Jonas, P. (1998) Functional and molecular differences between voltage-gated K^+ channels of fast-spiking interneurons and pyramidal neurons of rat hippocampus. *J. Neurosci.*, **18**, 8111–8125.
Martin-Caraballo, M. & Greer, J.J. (2000) Development of potassium conductances in perinatal rat phrenic motoneurons. *J. Neurophysiol.*, **83**, 3497–3508.
Mazza, E. Jr, Edelman, N.H. & Neubauer, J.A. (2000) Hypoxic excitation in neurons cultured from the rostral ventrolateral medulla of the neonatal rat. *J. Appl. Physiol.*, **88**, 2319–2329.
McCormick, D.A. (1991) Functional properties of a slowly inactivating potassium current in guinea pig dorsal lateral geniculate relay neurons. *J. Neurophysiol.*, **66**, 1176–1789.
McCormick, D.A. & Huguenard, J.R. (1992) A model of the electrophysiological properties of thalamocortical relay neurons. *J. Neurophysiol.*, **68**, 1384–1400.
McCrimmon, D.R., Monnier, A., Ptak, K., Zummo, G., Zhang, Z. & Alheid, G.F. (2001) Respiratory rhythm generation: preBotzinger neuron discharge patterns and persistent sodium current. In Poon, C.-S. & Kazemi, H. (eds), *Frontiers in Modeling and Control. of Breathing: Integration at Molecular, Cellular and Systems Levels*. Plenum/Kluwer Publications, New York, pp. 147–152.
Melton, J.E., Kadia, S.C., Yu, Q.P., Neubauer, J.A. & Edelman, N.H. (1996) Respiratory and sympathetic activity during recovery from hypoxic depression and gasping in cats. *J. Appl. Physiol.*, **80**, 1940–1948.
Pan, W.J., Osmanovic, S.S. & Shefner, S.A. (1995) Characterization of the adenosine A1 receptor-activated potassium current in rat locus ceruleus neurons. *J. Pharmacol. Exp. Ther.*, **273**, 537–544.
Pape, H.C. & Driesang, R.B. (1998) Ionic mechanisms of intrinsic oscillations in neurons of the basolateral amygdaloid complex. *J. Neurophysiol.*, **79**, 217–226.
Parkis, M.A., Pena, F. & Ramirez, J.M. (2002) The role of pacemaker neurons in the generation of different respiratory rhythms. *Program No. 362.5 2002 Abstracts Viewer/Itinerary Planner*, CD ROM. Society for Neuroscience, Washington, DC.
Pennartz, C.M., Bierlaagh, M.A. & Geurtsen, A.M. (1997) Cellular mechanisms underlying spontaneous firing in rat suprachiasmatic nucleus: involvement of a slowly inactivating component of sodium current. *J. Neurophysiol.*, **78**, 1811–1825.
Pierrefiche, O., Maniak, F. & Larnicol, N. (2002) Rhythmic activity from transverse brainstem slice of neonatal rat is modulated by nitric oxide. *Neuropharmacology*, **43**, 85–94.
Ramirez, J.M., Quellmalz, U.J.A. & Richter, D.W. (1996) Postnatal changes in the mammalian respiratory network as revealed by the transverse brainstem slice preparation of mice. *J. Physiol. (Lond.)*, **491**, 799–812.
Rekling, J.C. & Feldman, J.L. (1998) Pre-Bötzinger complex and pacemaker neurons: hypothesized site and kernel for respiratory rhythm generation. *Annu. Rev. Physiol.*, **60**, 385–405.
Remmers, J.E. (1998) Central neural control of breathing. In Altose, M.D. & Kawakami, Y. (eds), *Control of Breathing in Health and Disease*. Marcel Dekker, New York, pp. 1–40.
Rybak, I.A., St-John, W.M. & Paton, J.F.R. (2001) Models of neuronal bursting behavior: Implications for *in vivo* versus *in vitro* respiratory rhythmogenesis. In Poon, C.-S. & Kazemi, H. (eds), *Frontiers in Modeling and Control. of Breathing: Integration at Molecular, Cellular and Systems Levels*. Plenum/Kluwer Publications, New York, pp. 159–164.
Rybak, I.A., Paton, J.F.R., Rogers, R.F. & St-John, W.M. (2002) Generation of the respiratory rhythm: state-dependency and switching. *Neurocomputing*, **44–46**, 605–614.
Rybak, I.A., Ptak, K., Shevtsova, N.A. & McCrimmon, D.R. (2003) Sodium currents in neurons from the rostroventrolateral medulla of the rat. *J. Neurophysiol.*, **90**, in press.
Shao, X.M. & Feldman, J.L. (1997) Respiratory rhythm generation and synaptic inhibition of expiratory neurons in pre-Bötzinger complex: differential roles of glycinergic and gabaergic neural transmission. *J. Neurophysiol.*, **77**, 1853–1860.
Shevtsova, N.A., Ptak, K., McCrimmon, D.R. & Rybak, I.A. (2002) Study of sodium currents in neurons of pre-Bötzinger complex. *Program No. 173.5 2002 Abstracts Viewer/Itinerary Planner*, CD ROM. Society for Neuroscience, Washington, DC.
Smith, J.C. (1997) Integration of cellular and network mechanisms in mammalian oscillatory motor circuits. Insights from the respiratory oscillator. In Paul, S.G., Stein, P.S.G., Grillner, S., Selverston, A.I., Poggio, T. & Stuart, D.G. (eds), *Neurons, Networks, and Motor Behavior*. MIT Press, Cambridge, MA, pp. 97–104.
Smith, J.C., Butera, R.J., Koshiya, N., Del Negro, C., Wilson, C.G. & Johnson, S.M. (2000) Respiratory rhythm generation in neonatal and adult mammals: The hybrid pacemaker-network model. *Respir. Physiol.*, **122**, 131–147.
Smith, J.C., Ellenberger, H.H., Ballanyi, K., Richter, D.W. & Feldman, J.L. (1991) Pre-Bötzinger complex: a brainstem region that may generate respiratory rhythm in mammals. *Science*, **254**, 726–729.
Solomon, I.C. (2002) Modulation of gasp frequency by activation of pre-Bötzinger complex *in vivo*. *J. Neurophysiol.*, **87**, 1664–1668.
Solomon, I.C., Edelman, N.H. & Neubauer, J.A. (2000) Pre-Bötzinger complex functions as a central hypoxia chemosensor for respiration *in vivo*. *J. Neurophysiol.*, **83**, 2854–2868.
St-John, W.M. (1996) Medullary regions for neurogenesis of gasping: noeud vital or noeuds vitals? *J. Appl. Physiol.*, **81**, 1865–1877.
St-John, W.M. (1998) Neurogenesis of patterns of automatic ventilatory activity. *Prog. Neurobiol.*, **56**, 97–117.
St-John, W.M. & Paton, J.F.R. (2000) Characterizations of eupnea, apneusis and gasping in a perfused rat preparation. *Respir. Physiol.*, **123**, 201–213.
St-John, W.M. & Paton, J.F.R. (2002) Neurogenesis of gasping does not require inhibitory transmission using $GABA_A$ or glycine receptors. *Respir. Physiol. Neurobiol.*, **132**, 265–277.
St-John, W.M., Rybak, I.A. & Paton, J.F.R. (2002) Potential switch from eupnea to fictive gasping after blockade of glycine transmission and potassium channels. *Am. J. Physiol. (Integr. Comp. Physiol.)*, **283**, R721–R731.
Takakusaki, K. & Kitai, S.T. (1997) Ionic mechanisms involved in the spontaneous firing of tegmental pedunculopontine nucleus neurons of the rat. *Neuroscience*, **78**, 771–794.
Thoby-Brisson, M. & Ramirez, J.M. (2001) Identification of two types of inspiratory pacemaker neurons in the isolated respiratory network of mice. *J. Neurophysiol.*, **86**, 104–112.
Thompson, R.J. & Nurse, C.A. (1998) Anoxia differentially modulates multiple K^+ currents and depolarises neonatal rat adrenal chromaffin cells. *J. Physiol. (Lond.)*, **512**, 421–434.
Tryba, A.K., Pena, F. & Ramirez, J.M. (2003) Stabilization of bursting in respiratory pacemaker neurons. *J. Neurosci.*, **23**, 3538–3546.
Urbani, A. & Belluzzi, O. (2000) Riluzole inhibits the persistent sodium current in mammalian CNS neurons. *Eur. J. Neurosci.*, **12**, 3567–3574.
Völker, A., Ballanyi, K. & Richter, D.W. (1995) Anoxic disturbance of the isolated respiratory network of neonatal rats. *Exp. Brain Res.*, **103**, 9–19.
Xu, Z.J. & Adams, D.J. (1992) Resting membrane potential and potassium currents in cultured parasympathetic neurones from rat intracardiac ganglia. *J. Physiol. (Lond.)*, **456**, 405–424.